2-1-2012

Propagation of intense UV filaments and vortices.

Alexey Sukhinin

Recommended Citation

Sukhinin, Alexey. "Propagation of intense UV filaments and vortices.." (2012). https://digitalrepository.unm.edu/math_etds/46

Alexey Sukhinin

Candidate

Mathematics

Department

This dissertation is approved, and it is acceptable in quality and form for publication:

Approved by the Dissertation Committee:

Alejandro Aceves, Chairperson

Jean-Claude Diels

Stephen Lau

Pavel Lushnikov

Propagation of intense UV filaments and vortices

by

Alexey Sukhinin

B.S., Taurida National University, Ukraine, 2002
M.S., Mathematics, University of New Mexico, USA, 2005

DISSERTATION

Submitted in Partial Fulfillment of the
Requirements for the Degree of

Doctor of Philosophy
Mathematics

The University of New Mexico

Albuquerque, New Mexico

December, 2011

Dedication

To my parents Nickolay and Tatyana, for their support and help during all my life.

Acknowledgments

First of all I would like to thank my adviser Alejandro Aceves for his help, advice, patience and support throughout the whole period of writing this dissertation. I must acknowledge his professionalism and persistence as well as friendliness and ability to make people feel good. I'm very grateful to Jean-Claude Diels and Pavel Lushnikov for their valuable comments. Special thanks to Stephen Lau for providing me with computational resources from Center for Advanced Research Computing as well as many beneficial suggestions. I am very proud to have them in my dissertation committee. Also, I want to thank Sergey Dyachenko, Denis Silantyev and Taylor Dupuy for fun and interesting conversations on different issues in theoretical physics. I'm indebted to Christina Hall for reading and checking my mistakes. Finally I want to thank my parents, my sister and my nephew for understanding and support.

Propagation of intense UV filaments and vortices

by

Alexey Sukhinin

ABSTRACT OF DISSERTATION

Submitted in Partial Fulfillment of the
Requirements for the Degree of

Doctor of Philosophy
Mathematics

The University of New Mexico

Albuquerque, New Mexico

December, 2011

Propagation of intense UV filaments and vortices

by

Alexey Sukhinin

B.S., Taurida National University, Ukraine, 2002
M.S., Mathematics, University of New Mexico, USA, 2005

Ph.D., Mathematics, University of New Mexico, 2011

Abstract

The goal of this dissertation is to investigate the propagation of ultrashort high intensity UV laser pulses of order of nanoseconds in atmosphere. It is believed that they have a potential for stable and diffractionless propagation over the extended distances. Consequently, it creates a new array of applications in areas of communication, sensing, energy transportation and others. The theoretical model derived from Maxwell's equations represents unidirectional envelope propagation and plasma creation equations.

It was shown numerically through Newton's iterations that the stationary model permits the localized fundamental and vortex solutions. Discussion of the stability of steady states involves different approaches and their limitations. Finally, model equations are integrated numerically to study the dynamics of the beams in the

stationary model as well as nanosecond pulses in the full (3+1)D model using parallel computation.

Contents

List of Figures

Chapter 1

Introduction

High intensity laser pulses have been studied extensively in nonlinear media such as gases, liquids and solids. It was observed that they undergo highly nonlinear behavior during propagation. At high peak power, ultrashort pulses tend to self-focus, which limits realization of the pulse characteristics experimentally due to the possibility of the damage of the active laser medium. Development of the chirped pulse amplification technique by Gerard Mourou and Donna Strickland in 1985 expanded the range of pulse powers that the laser can produce [1, 2]. Using this technique it was possible to generate ultrashort pulses with intensities up to the order of 10^{23} W/cm^2 [3].

One of the attractive research directions in this field is atmospheric pulse propagation. It was observed in a number of experiments that high intensity laser beams tend to create their own self-guiding mechanism staying focused over the extended distances [4, 5, 6, 7, 8]. This type of propagation creates several promising applications. The exploitation of this phenomenon requires thorough understanding of the fundamental physical effects that come into play. One of them is diffraction, which is a linear effect and an intrinsic property of laser beam propagation. Transverse distribution of the electric field of the beam is usually approximated by the Gaussian function. The distance along the propagation direction, for which the beam width increases by a factor of $\sqrt{2}$, is called the Rayleigh range. It is defined as $\pi w_0^2/\lambda$, where λ is the wavelength and w_0 is the beam waist. Often the propagation distance of high power pulses is compared to this quantity.

Another effect is Kerr lensing, which is responsible for self-focusing of the beam [9, 10]. This phenomenon represents the change of the refractive index of air due to the exposure to the high intensity beam, i.e. $n = n_0 + n_2 I$, where n_2 is the nonlinear Kerr index and I is the intensity of the beam. Depending on the initial power, propagation of the beam may differ. At power $P_{cr} = \lambda^2/8\pi n_0 n_2$, diffraction is balanced with self-focusing. A beam with power less than P_{cr} diffuses in the transverse direction. If the initial power of the beam exceeds critical power P_{cr}, the self-focusing becomes the dominant effect leading the beam to the ultimate collapse at a finite distance [11, 12, 13, 14, 15].

It is known that traveling pulses with high intensities ionize the medium. The energy of a single photon is not enough to eject the electron from its orbit. Ionization takes place due to absorption of multiple photons at the same time. The liberated electrons form a plasma that defocuses the beam [16].

Extended self-guided propagation is a result of the balance between diffraction, self-focusing and plasma defocusing. The process can be described in the following manner. A pulse with an initial power more than critical starts to collapse due to the Kerr effect. The collapse represents an event when beam intensity increases and beam width decreases. At some point, intensity reaches the ionization threshold and electron plasma is created near the focal point. Multiphoton ionization becomes the dominant effect and arrests the collapse [17, 18]. Depending on the initial beam power this process may be highly dynamic, representing focusing-defocusing cycles [19]. Eventual decrease of power because of nonlinear losses breaks up the balance and the beam diffracts.

By convention, self-guided propagation of a laser beam over many Rayleigh ranges was named filamentation or filament propagation. Some authors also use the terms self-channeling, self-trapping or self-induced waveguide propagation. There is more precise definition of the filament by Couairon [12] who defines it as a "dynamic structure with intense core, that is able to propagate over extended distances much larger than the typical diffraction length while keeping a narrow beam size without the help of any external guiding mechanism". An even more restrictive definition describes filament as "a part of the propagation during which the pulse generates a column of weakly ionized plasma in its wake" [12].

A beam with an intense central core is not a prerequisite for filamentation. The possibility of filament propagation of high power localized optical vortices has been studded in a few papers [20, 21]. Such beams have doughnut or ring-shaped spatial distribution with zero intensity at the center and at infinity. Every vortex carries an integer that corresponds to the phase change around the ring. In the literature this number is called the topological charge of the vortex and represents the number of windings. It was observed that although subject to the azimuthal modulational instability, ring-like beams can constitute robust structures for many Rayleigh ranges. Vortex filaments in particular are interesting for application since they have an infinite number of states and can carry pulses for which critical power is much bigger than the critical power of the gaussian beam.

Apart from being able to transport high intensity pulses over extended distances, filaments were found to be very robust structures. They can even regenerate themselves beyond the location of a small obstacle-droplet, making propagation of the filaments stable under rainy or cloudy conditions [22, 23, 24, 25]. These properties can potentially find applications in areas of light direction and ranging (LIDAR), remote diagnostics and laser induced breakdown spectroscopy(LIBS) [26, 27, 28, 29, 30].

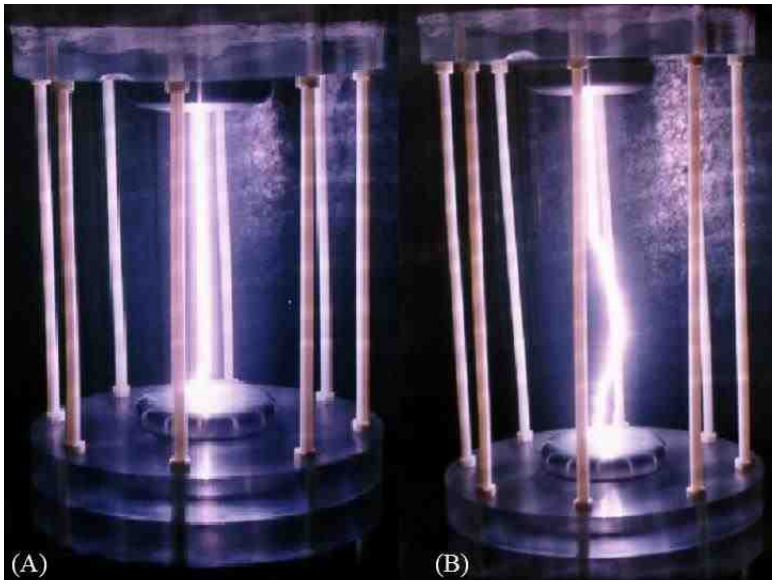

Figure 1.1: Electrical discharge triggered by filamentation at atmospheric pressure with focal positions (a) near mid-cell and (b) near the top electrode of the cell [32].

Ionization and creation of a plasma in the wake of high-intensity pulses has another remarkable application such as triggering and guiding of the electrical discharge [31, 32]. Figure 1.1 shows the experiment by Rambo et al. [32] of rectilinear propagation of electric discharge between two electrodes, using filamentation as a conducting channel. This effect is attractive for potential applications such as the contactless current transmission, lightning protection and directed energy [11].

In terms of mathematical modeling, dynamics of the filamentation is usually described by the unidirectional propagation equations. Providing the canonical description of slow varying pulse envelope propagation in weakly nonlinear media, the Nonlinear Schrodinger Equation(NLSE) and its variations gained the most popularity in the field. NLSE is considered to be the fundamental equation where only two effects are incorporated, namely diffraction and self-focusing. By adding additional terms and coupling equations, it is possible to construct relevant models for many propagation regimes. The validity of such models may break down as the pulse nears the collapse due to applicability restrictions to small amplitudes [33]. Although equations based on NLSE typically are not integrable in dimensions more than one, there are number of numerical methods that can be applied to find solutions. As a rule, (2+1)D models don't require heavy computational resources for integration over a few meters. To catch the full dynamics of the pulse in (3+1)D case, parallel computations can be used. Results from numerical simulations and experimental data have been shown to be in sufficient agreement.

Currently several groups are working in the area of ultrashort high-intensity laser pulses. Big contributions into the research came from the project called Teramobile organized in 1999 by the group of five laboratories located in Berlin, Dresden (Germany), Lyon, Palaiseau (France) and Geneva (Switzerland). They developed a unique mobile laser system based on the chirped pulse amplification technique that produces femtosecond pulses with peak power of a few terawatts [12].

Filamentation was observed in several experiments with femtosecond (fs) pulses in both infrared (IR) and ultraviolet (UV) wavelengths. Comparing the two regimes, it was detected that the IR filaments were obtained at much higher intensity but at shorter pulse duration than the UV [34]. A few ps UV pulses were the longest for which filamentation was found. The upper bound for the length of the pulse that can produce filament is determined by the time necessary for electrons to gain ionization energy of oxygen due to the inverse Bremsstrahlung. Plasma heating at this time results in breakdown of air. For IR filaments with a 100 μm diameter it happens around 1 ps. Since the rate of heating of electron plasma is proportional to the wavelength and intensity, filaments can potentially be produced with longer UV pulses.

High power UV pulses are especially interesting for long propagation. According to [35], UV filament loses only about 30-40 μJ per meter. This is much less than the nonlinear losses of IR filaments. By increasing pulse duration, the UV filaments created can be longer(possibly even of the order of kilometers) and contain more energy.

This dissertation is a theoretical examination of UV pulses of the duration of the order of nanoseconds. An ongoing experiment at the University of New Mexico has been conducted by professor Diels' group. Nd:YAG laser oscillator-amplifier system is utilized to generate pulses with quadrupled frequency. In order to obtain long UV pulses with predetermined energy stimulated Brillouin scattering is used for compression [36].

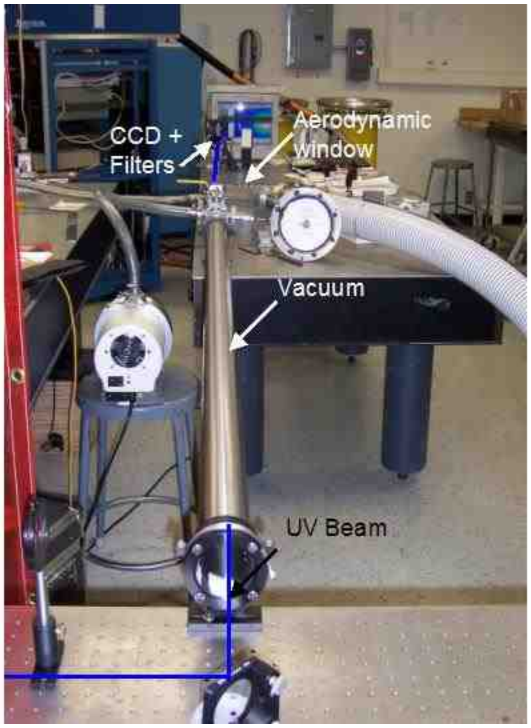

Figure 1.2: Experimental setup by Diels' group

Due to the space limitations of the lab, measurements of propagation distance of the filaments are bounded to the range of a few meters. The aerodynamic window, as it seen on Figure 1.2, is a special device that was developed to stabilize the starting position of the filament. Although generation of filaments using nanosecond pulses with a few Joule of energy is still under construction, filamentation within 4 meters from the aerodynamic window was observed using 200 ps pulses with energy 500 mJ at 266 nm.

After the general introduction of this dissertation, **chapter 2** provides the details of the mathematical model. Starting from Maxwell's equations it shows the derivation of the equation governing the nonlinear unidirectional propagation of a slowly varying wavepacket envelope of a UV laser pulse. Formulation of the plasma generation induced by the 3-photon ionization completes the model and the resulted coupled equations are presented with defined physical quantities.

Chapter 3 begins with examining the stationary propagation model where time dependence is neglected along with all possible losses. The nonlinear eigenvalue problem is obtained from the steady state equation and a brief discussion of uniformly distributed plane wave solutions is given. The chapter continues with the detailed description of the numerical method that is used to find families of localized standing filament profiles that vanish at infinity. With slight modification, the same method is used to obtain vortex steady state solutions for different values of the topological charge. These solutions are the main results of the chapter.

Chapter 4 addresses issues of stability of the localized solutions. The analysis starts with a semi-analytical approach. Propagation equations of the beam width are introduced using three different methods. The resulting equations are analyzed and the implication on propagation is discussed. Then, linear stability analysis is formulated and explored. This analysis includes the introduction of spatial perturbations, the setup of the spectral problem and the verification of Vakhitov-Kolokolov criterion. The discussion continues with the azimuthal instability of vortex stationary solutions via derivation of the growth rate formula. The chapter ends with the analysis of the spectral problem obtained from introducing spatiotemporal perturbations.

Chapter 5 describes numerical simulations of (2+1)D stationary and (3+1)D non-stationary models. A discussion of the results is provided.

The description of the numerical method that is used in the propagation model is given in **Appendix A**.

Chapter 2

The physical model

2.1 Derivation of propagation equation.

Since light is a form of electromagnetic field, we start our modeling with the classical theory based on Maxwell's equations [37, 38]

$$\begin{aligned}
\text{Gauss' law for electricity:} \quad \nabla \cdot \vec{D} &= \rho && (2.1)\\
\text{Gauss' law for magnetism:} \quad \nabla \cdot \vec{B} &= 0 && (2.2)\\
\text{Faraday's law:} \quad \nabla \times \vec{E} &= -\frac{\partial \vec{B}}{\partial t} && (2.3)\\
\text{Ampere-Maxwell law:} \quad \nabla \times \vec{H} &= \frac{\partial \vec{D}}{\partial t} + \vec{J} && (2.4)
\end{aligned}$$

where ρ and $\vec{J}$ are the electric charge and current densities.

The flux densities $\vec{D}$ and $\vec{B}$ related to electric and magnetic fields $\vec{E}$ and $\vec{H}$ through the complemented relations

$$\vec{D} = \varepsilon_0 \vec{E} + \vec{P} \tag{2.5}$$

$$\vec{B} = \mu_0 \vec{H} + \vec{M} \tag{2.6}$$

where $\vec{P}$ and $\vec{M}$ are the induced electric and magnetic polarization, and ε_0 and μ_0 are the vacuum permittivity and vacuum permeability. For a nonmagnetic medium, $\vec{M} = \vec{0}$. Now, taking curl of equation (2.3), using identity (2.4),(2.5) and (2.6) we obtain

$$\nabla \times \nabla \times \vec{E} = -\frac{1}{c^2}\frac{\partial^2 \vec{E}}{\partial t^2} - \mu_0 \frac{\partial^2 \vec{P}}{\partial t^2} - \mu_0 \frac{\partial \vec{J}}{\partial t} \tag{2.7}$$

where $1/c^2 = \varepsilon_0 \mu_0$. On the left hand side we use the vector identity

$$\nabla \times \nabla \times \vec{E} = \nabla(\nabla \cdot \vec{E}) - \nabla^2 \vec{E} = -\nabla^2 \vec{E} \tag{2.8}$$

where $\nabla \cdot \vec{E} = 0$, by divergence free assumptions [39]. After substituting (2.8) into (2.7) we have

$$\nabla^2 \vec{E} - \frac{1}{c^2}\frac{\partial^2 \vec{E}}{\partial t^2} = \mu_0 \left(\frac{\partial^2 \vec{P}}{\partial t^2} + \frac{\partial \vec{J}}{\partial t} \right). \tag{2.9}$$

Air can be considered to be a centro-symmetric medium with linear index n_0, where inversion symmetry is also present. Because of that, the polarization field can be expanded in power series of $\vec{E}$ with cubic being lowest order nonlinearity. The first term in the series corresponds to the linear polarization $\vec{P}_L$. Nonlinear polarization which is the rest of the expansion can be treated as a small perturbation to the linear since $|\vec{P}_{NL}| << |\vec{P}_L|$ [40].

In general, the linear polarization is related to the field through the dielectric susceptibility

$$\vec{P}_L = \epsilon_0 \int_{-\infty}^{\infty} \chi^{(1)}(t-\tau)\vec{E}(x,y,z,\tau)d\tau \tag{2.10}$$

while in the frequency domain, from the convolution theorem, is

$$\vec{\tilde{P}}_L = \epsilon_0 \chi^{(1)}(\omega)\vec{\tilde{E}}(\omega). \tag{2.11}$$

The linear refractive index is defined by $n_0^2(\omega) = 1 + \chi^{(1)}(\omega)$ and the wavenumber by dispersion relation $k(\omega) = \omega n(\omega)/c$. For further consideration we expand $k(\omega)$ in the Taylor series about the carrier frequency ω_0

$$k(\omega) = k(\omega_0) + k'(\omega_0)(\omega-\omega_0) + \sum_{n=2}^{\infty} \frac{1}{n!} k^{(n)}(\omega_0)(\omega-\omega_0)^n. \tag{2.12}$$

It is assumed that the field represents a beam propagating in one direction, namely in direction z. This is why in the slowly varying quasi-monochromatic approximation, it is useful to separate the rapidly varying part of the electric field by writing it in the form

$$\vec{E}(x,y,z,t) \quad = \hat{e}(\mathcal{E}(x,y,z,t)e^{i(k_0 z - w_0 t)} + c.c.) \tag{2.13}$$

where $\hat{e}$ is the polarization unit vector, $\mathcal{E}$ is the slowly varying complex amplitude and

$k_0 = k(\omega_0)$. The concept of slowly varying amplitude $\mathcal{E}$ means that $|\partial\mathcal{E}/\partial z| << k_0|\mathcal{E}|$ and $|\partial\mathcal{E}/\partial t| << \omega_0|\mathcal{E}|$.

The amplitude $\mathcal{E}$, in turn, can be represented as a Fourier integral

$$\mathcal{E}(x,y,z,t) = \int_{-\infty}^{\infty} \hat{\mathcal{E}}(x,y,z,\omega)e^{-i\omega t}d\omega \tag{2.14}$$

so the linear part (LP) of equation (2.9) can be written in the form

$$LP = e^{i(k_0 z - w_0 t)}\left[\left(\frac{\partial}{\partial z} + ik_0\right)^2 \mathcal{E} + \triangle_\perp \mathcal{E} + \int_{-\infty}^{\infty} k^2(\omega_0+\omega)\hat{\mathcal{E}}(\omega)e^{-i\omega t}d\omega\right] \tag{2.15}$$

where $\triangle_\perp$ stands for transverse laplacian. Using expansion (2.12) and keeping terms up to second order, the following is obtained

$$LP = e^{i(k_0 z - w_0 t)}\left[\frac{\partial^2\mathcal{E}}{\partial z^2} + 2ik_0\frac{\partial\mathcal{E}}{\partial z} + \triangle_\perp\mathcal{E} + 2ik_0k_0'\frac{\partial\mathcal{E}}{\partial t} - (k_0'^2 + k_0k_0'')\frac{\partial^2\mathcal{E}}{\partial t^2}\right]. \tag{2.16}$$

It is also convenient to write the equation in a frame moving with the group velocity of the pulse. This can be achieved by making a transformation $t \rightarrow t - k_0'z$ and $z \rightarrow z$. As for second derivatives

$$\frac{\partial^2\mathcal{E}}{\partial z^2} - k_0'^2\frac{\partial^2\mathcal{E}}{\partial t^2} = \left(\frac{\partial}{\partial z} - k_0'\frac{\partial}{\partial t}\right)\left(\frac{\partial}{\partial z} + k_0'\frac{\partial}{\partial t}\right)\mathcal{E} << \mathcal{E}. \tag{2.17}$$

The equation (2.16) can be reduced to

$$LP = e^{i(k_0 z - w_0 t)}\left[2ik_0\frac{\partial\mathcal{E}}{\partial z} + \triangle_\perp\mathcal{E} - k_0k_0''\frac{\partial^2\mathcal{E}}{\partial t^2}\right]. \tag{2.18}$$

The nonlinear part (NP) of equation (2.9) consists of the nonlinear polarization and current density that is driven by the optical field. Since $\vec{P}_{NL}$ acts as perturbation of $\vec{P}_L$, higher order terms of nonlinear polarization are neglected except the dominant $\chi^{(3)}$, which corresponds to the optical Kerr effect. Now, if it is assumed that the response of the medium is instantaneous, then the nonlinear polarization can be simplified to

$$\vec{P}_{NL} = \epsilon_0 \chi^{(3)} (\vec{E} \cdot \vec{E}) \vec{E} \simeq 2 n_0 n_2 \epsilon_0 I \vec{E}. \tag{2.19}$$

Here, n_2 is the self-focusing index and I is the laser intensity, defined as $I = \frac{n_0}{2\eta_0} |\mathcal{E}|^2$, where $\eta_0 = \sqrt{\mu_0/\epsilon_0}$ is the characteristic impedance of the vacuum.

In general, $\chi^{(3)}$ includes the contribution of molecular vibrations and rotations. Although Raman contribution is important for ultrashort pulses, this is not the case for this work which assumes long UV pulses.

The model of plasma formation includes both multiphoton ionization and losses due to response of produced charges to the optical field. While IR pulses are required to have 8-10 photons to liberate the electron from a molecule, simultaneous absorption of 3-4 photons for UV pulses is enough. Ionization potential of oxygen is lower compared to nitrogen. Hence, we can neglect ionization of nitrogen, due to the small contribution. It follows that the number of electrons in the plasma is small relative to the number of neutral molecules.

Schwarz et al.[35] set up the time scale under which current research is defined. While the upper limit was established by inverse Bremsstrahlung, the lower limit was defined by the time of plasma creation. As a result, the range of pulses duration to be considered is between a few to 200 nanoseconds. In this range we can neglect a second ionizing mechanism which occurs due to plasma heating by the laser field. The losses of plasma occur when free electrons attach to positive ions producing neutral molecules of oxygen. Another loss term in the plasma evolution equation can be included due to the attachment of electrons to neutral molecules. The equation governing free electron generation takes the form

$$\frac{\partial N_e}{\partial t} = \sigma^{(3)} N_0 I^3 - \beta_{ep} N_e^2 - \gamma N_e \tag{2.20}$$

where N_e is the density of the electron plasma, $\sigma^{(3)}$ the 3d order multiphoton ionization coefficient, β_{ep} the recombination coefficient and γ the electron-oxygen attachment coefficient.

To complete the model we need to examine current density $\vec{J}$, which consists of free electron density $\vec{J}_e$ and additional ionization current $\vec{J}_{MPA}$, which stands for multiphoton absorption, i.e.

$$\vec{J} = \vec{J}_e + \vec{J}_{MPA}. \tag{2.21}$$

Following the photo-ionization theory, the electron plasma is considered as a fluid and can be modeled through collective velocity $\vec{v}_e$

$$\frac{\partial}{\partial t}\vec{v}_e = -\frac{e}{m_e}\vec{E} - \nu \vec{v}_e \tag{2.22}$$

where m_e is the electron mass, e the elementary charge and ν the electron collision frequency [41, 42].

Since motion of plasma electrons occurs in the optical field with much lower frequency than ω_0, we can separate fast and slow oscillations and eliminate the fast part

$$v_{LF} \simeq -\frac{e\mathcal{E}}{m_e(\nu - i\omega_0)}. \tag{2.23}$$

Free electron current density $\vec{J}_e = -eN_e\vec{v}_e$ can be also decomposed to fast and slow oscillation terms, where the low frequency contribution is given by

$$\frac{\partial}{\partial t}J_{e_{LF}} \simeq -i\frac{\omega_0 e^2 N_e \mathcal{E}}{m_e(\nu - i\omega_0)} \approx \left(1 - i\frac{\nu}{\omega_0}\right)\frac{e^2}{m_e}N_e\mathcal{E}. \tag{2.24}$$

The last approximation is due to the fact that $\nu << \omega_0$. The current in (2.21), which accounts for dissipation of power necessary for multiphoton ionization, can be expressed through electric field [42]

$$\frac{\partial}{\partial t}J_{MPA_{LF}} = -i\frac{\beta^{(3)}k_0 n_0^2}{4\mu_0\eta_0^2}|\mathcal{E}|^4\mathcal{E}. \tag{2.25}$$

If equations (2.9), (2.18),(2.19) and (2.20) are combined with equations (2.21),(2.24) and (2.25) along with cancelation of $e^{i(k_0 z - \omega_0 t)}$, we immediately get

$$2ik_0\frac{\partial\mathcal{E}}{\partial z} + \nabla_\perp^2\mathcal{E} + k_0^2\frac{n_2}{\eta_0}|\mathcal{E}|^2\mathcal{E} + -k_0^2\frac{e^2}{m_e\omega_0^2\epsilon_0 n_0^2}(1 - i\frac{\nu}{\omega_0})N_e\mathcal{E} + i\frac{\beta^{(3)}k_0 n_0^2}{4\eta_0^2}|\mathcal{E}|^4\mathcal{E} = 0$$

and

$$\frac{\partial N_e}{\partial t} = \sigma^{(3)}N_0\frac{n_0^3}{8\eta_0^3}|\mathcal{E}|^6 - \beta_{ep}N_e^2 - \gamma N_e. \tag{2.26}$$

Table 2.1: Typical physical parameters. [35]

Parameter	Symbol	Value	Units
Linear index	n_0	1.000259	
Self-focusing index	n_2	7.8×10^{-23}	m^2/W
Wavelength	λ	266×10^{-9}	m
Three-photon absorption cross section	$\sigma^{(3)}$	3.0×10^{-41}	$\mathrm{m}^6\mathrm{s}^2/\mathrm{J}^3$
Density of neutral oxygen	N_0	5.4×10^{24}	$1/\mathrm{m}^3$
Recombination coefficient	β_{ep}	1.3×10^{-14}	m^3/s
Attachment coefficient	γ	1.5×10^{8}	1/s
Electron collision frequency	ν	1.67×10^{10}	1/s
MPI coefficient	$\beta^{(3)}$	3.9×10^{-34}	$\mathrm{m}^3/\mathrm{W}^2$
Vacuum permeability	μ_0	$4\pi \times 10^{-7}$	$\mathrm{mkg}/\mathrm{A}^2\mathrm{s}^2$
Vacuum permittivity	ϵ_0	8.854×10^{-12}	$\mathrm{A}^2\mathrm{s}^4/\mathrm{m}^3\ \mathrm{kg}$
Electron charge	e	1.602×10^{-19}	C
Electron mass	m_e	9.109×10^{-31}	kg

Chapter 3

Stationary solutions

3.1 The reduced model.

In the model derived in the previous chapter, UV filamentation is very sensitive to the initial conditions. Since we are interested in answering the question about the existence of pulses that maintain their shape over a long distance, this chapter studies the stationary model. This means that all terms with time derivatives will be dropped. Here, we consider the ideal case where all the loss terms are neglected in the field envelope propagation equation, otherwise the beam would continuously decrease due to the losses. The following equations are under consideration

$$2ik_0\frac{\partial \mathcal{E}}{\partial z} + \nabla_\perp^2 \mathcal{E} + k_0^2 \frac{n_2}{\eta_0}|\mathcal{E}|^2\mathcal{E} - k_0^2 \frac{e^2}{m_e \omega_0^2 \epsilon_0 n_0^2} N_e \mathcal{E} = 0 \tag{3.1}$$

$$\sigma^{(3)} N_0 \frac{n_0^3}{8\eta_0^3}|\mathcal{E}|^6 - \beta_{ep} N_e^2 - \gamma N_e = 0. \tag{3.2}$$

Based on experimental observations, equation (3.1) will be considered with assumption of cylindrical symmetry. The equilibrium electron density can be expressed explicitly in equation (3.2)

$$N_{e_S} = \sqrt{\frac{\gamma^2}{4\beta_{ep}^2} + \frac{\sigma^{(3)} N_0 n_0^3 |\mathcal{E}|^6}{8\beta_{ep}\eta_0^3}} - \frac{\gamma}{2\beta_{ep}}. \tag{3.3}$$

From the physical point of view, it is possible to neglect the last term in equation (3.2). Schwarz and Diels [35] argued that the inverse of γ will not be of any effect during a pulse duration of a few nanoseconds. Theoretically, it shifts the validity of the model to the range from 200 picoseconds to a few nanoseconds. This assumption simplifies the analysis of the equation because the nonlinearity becomes of power order and makes it possible to use the full Hamiltonian structure machinery. We investigate both scenarios along the way, although some approaches can be applicable only to cubic-quartic nonlinearity.

After substituting (3.3) into equation (3.1), a single 2D field equation emerges. To obtain nondimensional equations, the dimensionless quantities are defined in the following way

$$\mathcal{E} \to \psi\mathcal{E}_0,\ r \to\ r r_0,\ z \to\ z z_0$$

where $\mathcal{E}_0$, r_0 and z_0 denote dimensional constants with units of electric field, length and length respectively. Using dimensionless variables, equation (3.1) becomes

$$\begin{aligned} i\frac{2k_0 r_0^2}{z_0}\frac{\partial\psi}{\partial z} + \frac{1}{r}\frac{\partial\psi}{\partial r} + \frac{\partial^2\psi}{\partial r^2} + \frac{1}{r^2}\frac{\partial^2\psi}{\partial^2\theta} + k_0^2\mathcal{E}_0^2 r_0^2\frac{n_2}{\eta_0}|\psi|^2\psi \\ -k_0^2\frac{e^2 r_0^2}{m_e\omega_0^2\epsilon_0 n_0^2}\left(\sqrt{\frac{\gamma^2}{4\beta_{ep}^2} + \frac{\sigma^{(3)} N_0 n_0^3 \mathcal{E}_0^6 |\psi|^6}{8\beta_{ep}\eta_0^3}} - \frac{\gamma}{2\beta_{ep}}\right)\psi = 0. \end{aligned} \tag{3.4}$$

There are several options for defining the dimensional variables and coefficients. Usually the electric field is normalized with respect to self focusing index and higher order nonlinearities, so these quantities are defined in the following way

$$r_0 = \left(\frac{\eta_0}{k_0^2 \mathcal{E}_0^2 n_2}\right)^{1/2}, \mathcal{E}_0 = \left(\frac{m_e \omega_0^2 \epsilon_0 n_2}{e^2} \sqrt{\frac{8 n_0 \beta_{ep} \eta_0}{\sigma^{(3)} N_0}}\right), z_0 = 2 k_0 r_0^2, \mu = \frac{\gamma k_0^2 e^2 r_0^2}{2 \beta_{ep} m_e \omega_0^2 \epsilon_0 n_0^2}.$$

The equation (3.4) becomes

$$i\frac{\partial \psi}{\partial z} + \frac{1}{r}\frac{\partial \psi}{\partial r} + \frac{\partial^2 \psi}{\partial r^2} + \frac{1}{r^2}\frac{\partial^2 \psi}{\partial^2 \theta} + |\psi|^2\psi - F(|\psi|^2)\psi = 0 \tag{3.5}$$

where $F(|\psi|^2) = \sqrt{\mu^2 + |\psi|^6} - \mu$, with $\mu = 4.6$ or $F(|\psi|^2) = |\psi|^3$. From now on the former function is defined as $F_1(|\psi|^2)$ and the latter as $F_2(|\psi|^2)$.

3.2 Nonlinear eigenvalue problem.

To construct a steady state solution, we look for a solution of the following form $\psi(r, \theta, z) = \psi(r) e^{i\Lambda z + im\theta}$, where $\psi(r)$ is real radially symmetric profile of amplitude, $\Lambda > 0$ is a propagation constant and m is an integer. Notice that Λ is non-dimensional with the same scale as z. The substitution of the above ansatz into the equation (3.5) yields a boundary value problem.

$$-\Lambda\psi + \frac{1}{r}\frac{\partial \psi}{\partial r} + \frac{\partial^2 \psi}{\partial r^2} - \frac{m^2}{r^2}\psi + \psi^3 - F(\psi^2)\psi = 0 \tag{3.6}$$
$$\psi'(0) = 0, \;\; \psi(\infty) = 0.$$

Equation (3.6) can be treated as an eigenvalue problem with eigenvalue Λ and eigenfunction ψ. First we concentrate on the fundamental ground state solution which does not carry any topological charge, i.e. $m = 0$ in (3.6). Then we will consider stationary vortex solutions for different nonzero charges. The solutions ψ we look for are localized in space, which later can be interpolated onto an xy-plane.

There are several methods that can be utilized to solve this boundary value problem. One of them is the variational approach. This method uses trial function in order to find the main characteristics of the beam, i.e. beam width and peak amplitude. Although it provides relatively good explicit approximation, it has a disadvantage of assuming that the solution has the shape of the predetermined trial function.

The numerical approximation is another approach. Typically, boundary value problems can be successfully solved by shooting or using finite difference methods. The shooting method is known for its speed and adaptivity because it changes the boundary value problem to the initial value problem (IVP). Unfortunately, it is not as robust as the finite difference method because it can suffer from ill-conditioning of the IVP. The choice was to employ the finite difference scheme along with Newton's iterations.

3.2.1 Plane wave solutions.

Before going into the discussion of radially dependent profiles, we consider the simplest solutions of the given problem, which assume constant amplitude. These solutions are called plane wave solutions

$$\psi = \psi_s e^{i\Lambda z + im\theta}. \tag{3.7}$$

Substituting (3.7) into equation (3.5), we derive an implicit form for the solution

$$-\Lambda - \frac{m^2}{r^2} + \psi_s^2 - F(\psi_s^2) = 0.$$

Figure 3.1 shows example of solutions $\psi_s(r = r_m)$ of the above equation with mean radius $r_1 = 4.5$.

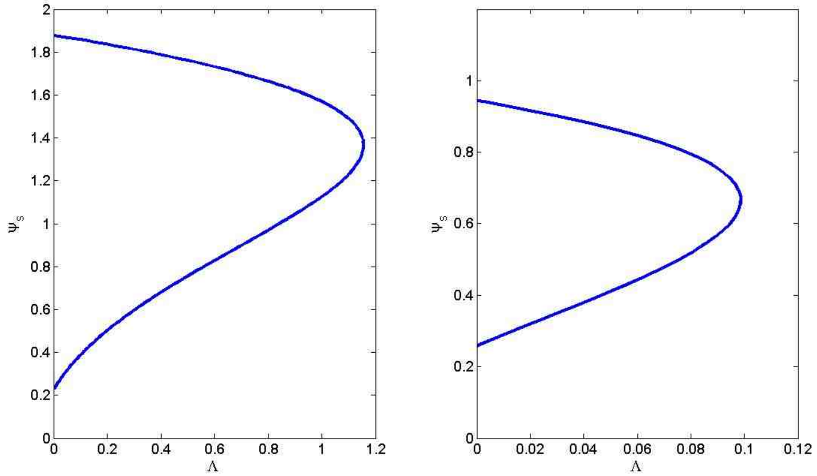

Figure 3.1: Plane wave solutions for m=1; (left)$F(\psi_s^2) = F_1(\psi_s^2)$, (right)$F(\psi_s^2) = F_2(\psi_s^2)$

3.2.2 Fundamental solutions.

If $F(\psi^2) = 0$, equation (3.6) becomes

$$-\Lambda\psi + \frac{1}{r}\frac{\partial \psi}{\partial r} + \frac{\partial^2 \psi}{\partial r^2} + \psi^3 = 0. \tag{3.8}$$

This is a well-known nonlinear eigenvalue problem with ground state solution, often called Townes soliton [43]. Townes profile assumes symmetric localized shape in radial dimension. In fact, equation (3.8) produces an infinite family of Townes solitons of the form $\sqrt{\Lambda}\psi(\sqrt{\Lambda}r)$ with the same power and different beam widths. Each profile is associated with corresponding eigenvalue Λ.

Having critical power, Townes is the unstable equilibrium of Nonlinear Schrodinger Equation in 2D. It is a borderline between blowup type and spreading-to-zero solutions. Initial beams that have more power than Townes will approach singularity at a finite distance. Those with less power will spread in the transverse dimension. In the present context, $F(\psi^2) = 0$ corresponds to the case when no plasma is present in the stationary model (3.6). The critical power for self-focusing of the equation (3.8) is

$$\int_0^\infty \psi(r)^2 r dr = P_{cr} \cong 1.862. \tag{3.9}$$

The Hamiltonian of equation (3.8) vanishes at Townes soliton solution

$$H(\psi(r)) = \int |\nabla_\perp \psi|^2 dr - \frac{1}{2}\int |\psi|^4 dr = 0. \tag{3.10}$$

These results were checked to confirm the validity of the numerical method described below.

Construction of the stationary solutions of equation (3.6) starts with the second order central difference discretization. Notice that at zero it is impossible to implement discrete laplacian. Taking into account that bound states are smooth and $\psi_r(0) = 0$, it is possible to eliminate singularity by observing that $\frac{1}{r}\psi_r(r) \approx \psi_{rr}(r)$ for small r.

In the discrete form the equation at zero becomes

$$4 \cdot \frac{\psi_1 - \psi_0}{h^2} + \psi_0^3 - F(\psi_0^2) = \Lambda \psi_0 \tag{3.11}$$

where due to the fact that the solution is radially symmetric, relation $\psi_1 = \psi_{-1}$ was used.

In order to implement boundary condition at infinity, Townes asymptotic behavior is assumed, i.e. $\psi(r) \approx A_R r^{-1/2} e^{-r}$, where $A_R \cong 3.52$, $r \gg 1$. If the numerical window is wide enough, it was observed that the value of the solution is substantially small for large r. In this case, simply assigning zero to $\psi(r)$ on the right boundary also produces the same result.

To solve system of nonlinear equations, Newton's iterations along with the continuation method are used. The continuation result will be used later in the stability chapter. The numerical algorithm of Newton's method was implemented with the following scheme

```
Step1. Let $(\Lambda, \psi^{(0)})$ be the initial guess, $j = 0$
Step2. while $||R(\psi^{(j)})|| > tolerance$
Step3. $\psi^{(j+1)} = \psi^{(j)} - J(\psi^{(j)})^{-1} R(\psi^{(j)})$
Step4. $j = j + 1$
Step5. end
```

where *tolerance* $= 10^{-7}$, J is the Jacobian matrix of R and function $R(\psi) = A\psi + f(\psi^2)$, where

$$A = \frac{1}{h^2}\begin{pmatrix} -4-\Lambda & 4 & & & & & \\ \frac{1}{2} & -2-\Lambda & \frac{3}{2} & & & & \\ & \frac{3}{4} & -2-\Lambda & \frac{5}{4} & & & \\ & & & & & & \\ & & & & \frac{2n-5}{2n-4} & -2-\Lambda & \frac{2n-3}{2n-4} \\ & & & & & \frac{2n-3}{2n-2} & -2-\Lambda \end{pmatrix}$$

and

$$f(\psi^2) = \begin{pmatrix} \psi_0^3 - F(\psi_0^2)\psi_0 \\ \psi_1^3 - F(\psi_1^2)\psi_1 \\ \cdots \\ \psi_{n-1}^3 - F(\psi_{n-1}^2)\psi_{n-1} \end{pmatrix}$$

where n is the number of points on the grid. Notice that only the nonlinear part will be updated at each iteration in the numerical implementation.

To obtain $J(\psi^{(j)})^{-1}R(\psi^{(j)})$, the Thomas algorithm is applied. This is a procedure that solves tridiagonal systems of linear equations by LU decomposition. This algorithm requires only $O(n)$ operations and doesn't utilize storage for full $n \times n$ matrix. The function in Matlab was defined as TRIDAG$(a, b, c, R(\psi^{(j)}))$ [44]. Here, a, b and c are vectors containing subdiagonal, diagonal and superdiagonal elements of $J(\psi^{(j)})$.

For convergence of the iterations, it is crucial to choose an initial guess $(\Lambda, \psi(r))$ close enough to the solution. Although Gaussian is a relatively good approximation of the Townes soliton, the guess was Townes in the form of a data vector that corresponds to appropriate Λ. After finding the first solution for the given Λ, this solution is used as an initial guess in Newton's iterations for $\Lambda + h$, where h is a small quantity. It was observed that this continuation has the following range $\Lambda \in [0.01, 0.36]$ for F_1 nonlinearity and $\Lambda \in [0.01, 0.103]$ for F_2. Figure 3.2 shows stationary solution corresponding to $\Lambda = 0.205$ of F_1 nonlinearity. Notice that steady states are well approximated by gaussian beams.

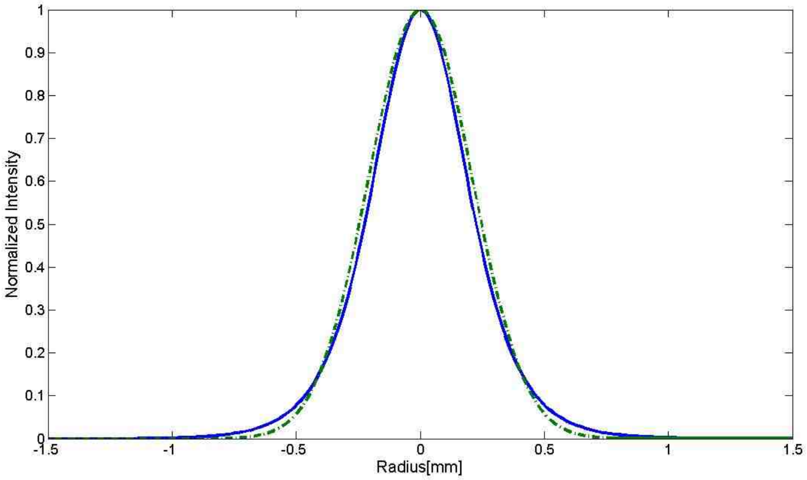

Figure 3.2: Comparison between numerically obtained steady state profile(solid) at $\Lambda = 0.205$ and gaussian beam(dot-dashed) $A_0^2 e^{-2r^2/\omega_0^2}$ with power 400MW.

3.2.3 Vortex solutions.

Optical vortex represents a field that exhibits radial symmetry in the form a ring and zero intensity at the center. In the stationary model (3.6), steady state vortex solutions correspond to the case when topological charge m is nonzero.

The numerical approach of finding the stationary vortices is the same as for the fundamental solution. The only difference is the discretization of the equation at zero. In the case of the vortex equation we have an additional term in the laplacian that blows up at zero. Knowing that $\psi(0) = 0$, observe $\frac{1}{r^2}\psi(r) \approx \frac{\psi_{rr}(r)}{2}$ when r is small. Below is the difference equation corresponding to the zero boundary

$$(4 + m) \cdot \frac{\psi_1 - \psi_0}{h^2} + \psi_0^3 - F(\psi_0^2) = \Lambda\psi_0. \tag{3.12}$$

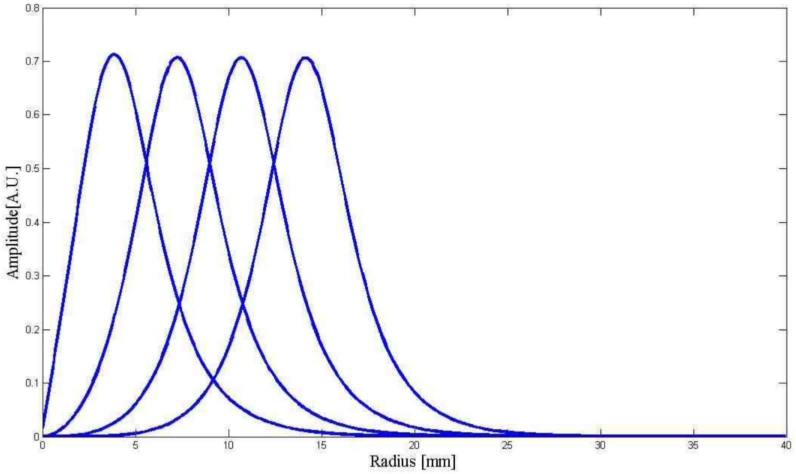

Figure 3.3: Distribution of stationary vortex solutions for $m = 1, 2, 3, 4$ at $\Lambda = 0.165$

As an initial guess the stationary profile obtained from equation (3.8) is used. As an example, for $F_1(|\psi|^2)$ nonlinearity, convergence is observed on the interval $\Lambda \in [0.06, 0.44]$ for $m = 1$. By increasing the numerical window it is possible to obtain solutions with larger m. Figure 3.3 shows distribution of stationary vortex solutions for F_1 nonlinearity with four different topological charges. Notice that for larger m the radius and power increase, thus making it harder to realize experimentally.

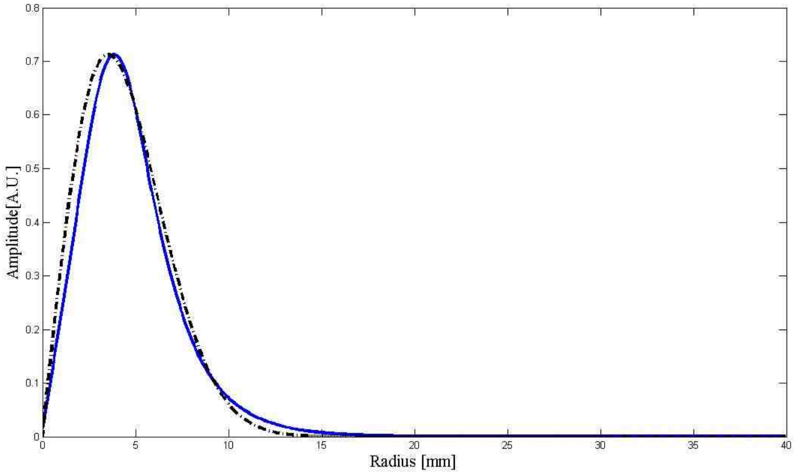

Figure 3.4: Comparison of numerical solution(solid) for m=1 and approximation(dot-dashed) $A_0 r e^{-r^2/\omega_0^2}, A_0 = 0.33, \omega_0 = 4$

Chapter 4

Stability analysis

Stability analysis of nonlinear waves is one of the most important issues in modeling real physical experiments. Noise, turbulence, errors in measurements and other small effects can contribute to deviations from the exact equilibrium. Usually direct numerical computations are performed in order to compare theory with experiment, but it is still not convincing without the analysis of stability properties against different perturbations.

The main goal of this chapter is to examine stability of the stationary ground-state solutions found in the previous chapter. The analysis is divided into two parts. In the first part of the chapter a semi-analytical approach is used. This approach doesn't exactly deal with the stationary solutions, but rather with gaussian approximations. Some of the methods are limited to the stationary equation with cubic-quartic nonlinearity only. In the second part of the chapter, analysis is done directly to steady states.

4.1 Semi-analytical approach.

Several semi-analytical methods can be used to study the ultrashort pulses in the air. Here, a variational [45, 46, 47] and parabolic approximation methods [35] are employed. The idea behind these methods is to describe the propagation of the main characteristics of the beam by using an appropriate trial function. It is assumed however, that the shape of the pulse profile is preserved, which imposes a limitation on the produced models.

Simple evolution equations for the beam width and power are the results of applying these methods. Although analysis based just on this equations may be superficial, approximate evaluation of the beam propagation can be obtained.

4.1.1 Gaussian Trial Function.

This method will be applied to equation (3.5) with cubic-quartic nonlinearity. The Lagrangian $\mathcal{L}$ corresponding to this problem is defined in the following way

$$\mathcal{L} = \frac{i}{2}\left(\psi^*\frac{\partial\psi}{\partial z} - \psi\frac{\partial\psi^*}{\partial z}\right) - \left|\frac{\partial\psi}{\partial r}\right|^2 + \frac{1}{2}|\psi|^4 - \frac{2}{5}|\psi|^5. \tag{4.1}$$

A suitable trial function corresponding to gaussian beam is given by

$$\psi(r,z) = A(z)e^{-\left(\frac{r^2}{\omega^2(z)}+iC(z)r^2+i\phi(z)\right)} \tag{4.2}$$

where parameters are amplitude A, beam width ω, wave curvature C and phase ϕ. Substitution (4.2) into (4.1) produces

$$\mathcal{L} = A^2(r^2C' + \phi')e^{-2r^2/\omega^2} - 4A^2r^2\left(\frac{1}{\omega^4} + C^2\right)e^{-2r^2/\omega^2} + \frac{1}{2}A^4e^{-4r^2/\omega^2} \\ -\frac{2}{5}A^5e^{-5r^2/\omega^2}. \tag{4.3}$$

After averaging over r, the reduced Lagrangian is given

$$< \mathcal{L} >= \int_0^\infty \mathcal{L} r dr = \alpha_1 A^2\phi' + \alpha_2 A^2\left(C' - \frac{4}{\omega^4} - 4C^2\right) + \alpha_3 A^4 - \alpha_4 A^5 \tag{4.4}$$

where $\alpha_1(\omega) = 2^{-2}\omega^2$, $\alpha_2(\omega) = 2^{-3}\omega^4$, $\alpha_3(\omega) = 2^{-4}\omega^2$ and $\alpha_4(\omega) = 5^{-2}\omega^2$.

To obtain Euler-Lagrange equations, the reduced Lagrangian is varied with respect to the parameters A^2, ω, ϕ and C.

Variation with respect to A^2:

$$\phi' + \frac{\omega^2}{2}\left(C' - \frac{4}{w^4} - 4C^2\right) + \frac{1}{2}A^2 - \frac{2}{5}A^3 = 0. \tag{4.5}$$

Variation with respect to ω:

$$\phi' + \omega^2\left(C' - \frac{4}{\omega^4} - 4C^2\right) + \frac{1}{4}A^2 - \frac{4}{25}A^3 = 0. \tag{4.6}$$

Variation with respect to ϕ:

$$\frac{\partial}{\partial z}\left(\omega^2 A^2\right) = 0. \tag{4.7}$$

Variation with respect to C:

$$8\omega^4 A^2 C + \frac{\partial}{\partial z}\left(\omega^4 A^2\right) = 0. \tag{4.8}$$

Equation (4.7) gives the initial conditions on the beam waist and amplitude of the gaussian function

$$A(z)\omega(z) = const = A(0)\omega(0). \tag{4.9}$$

After using simple algebra, the final equation for the beam waist is obtained

$$\frac{d^2\omega}{dz^2} = \frac{16 - 2A_0^2\omega_0^2}{\omega^3} + \frac{48\omega_0^3 A_0^3}{25}\frac{1}{\omega^4}. \tag{4.10}$$

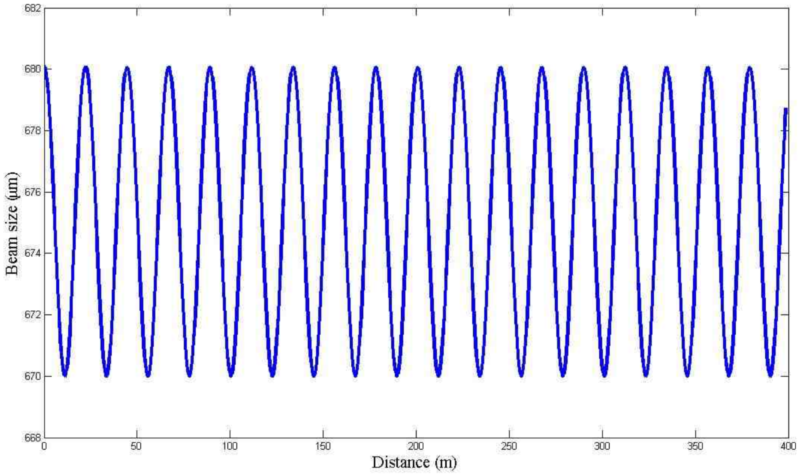

Figure 4.1: Propagation of the width of 380MW gaussian beam.

Equation (4.10) is solved numerically using Matlab ODE45 solver. Figure 4.1 shows oscillatory behavior of the gaussian beam with power 380MW. The initial conditions are taken from the gaussian approximation of the fundamental stationary solution of equation (3.5) with $F_2(|\psi|^2)$ nonlinearity that corresponds to $\Lambda = 0.063$.

Parabolic approximation method.

Despite similarity, the parabolic approximation method differs from the variational approach since a gaussian profile is substituted directly into the propagation equation. Evolution equations are obtained after expansion of the gaussian into the Taylor series near zero radius, making the main emphasis of this approach on the center of the beam. Taking ansatz

$$\psi(r,z) = A_0 \frac{\omega_0}{\omega(z)} e^{-\left(\frac{r^2}{\omega^2(z)} + i\frac{r^2}{2R(z)} + i\phi(z)\right)} \tag{4.11}$$

into equation (3.5) with $F_1(|\psi|^2)$ nonlinearity and using parabolic approximation

$$e^{\frac{-\alpha r^2}{\omega^2}} = 1 - \alpha \frac{r^2}{\omega^2} \tag{4.12}$$

two equations are obtained after keeping only leading order terms and equating real and imaginary parts

$$2r^2 \frac{w'(z)}{w(z)^3} - \frac{w'(z)}{w(z)} - \frac{2}{R(z)} + \frac{4r^2}{w(z)^2 R(z)} = 0 \tag{4.13}$$

$$-\frac{1}{2}\frac{r^2 R'(z)}{R(z)^2} + \phi'(z) - \frac{4}{w(z)^2} + \frac{4r^2}{w(z)^4} - \frac{r^2}{R(z)^2} + \frac{A^2}{w(z)^2} - \frac{2A^2 r^2}{w(z)^4} - \frac{\sqrt{\mu^2 w(z)^6 + A^6}}{w(z)^3} + \frac{3A^6 r^2}{\sqrt{\mu^2 w(z)^6 + A^6}\, w(z)^5} + \mu = 0. \tag{4.14}$$

The beam waist evolution equation follows after combining the terms with r^2 and simple algebraic manipulations

$$\frac{d^2w}{dz^2} = \frac{16 - 8A_0^2\omega_0^2}{w^3(z)} + \frac{12A_0^6\omega_0^6}{w^4\sqrt{\mu^2\omega^6 + A_0^6\omega_0^6}}. \tag{4.15}$$

However, equation (4.15) is only approximately correct. If $\mu \to \infty$, equation (3.5) becomes Nonlinear Schrodinger Equation and the second term on the right-hand side of equation (4.15) is zero. Simple diagnostics shows that the critical power for collapse event between NLSE and (4.15) differs by a factor 4. This can also be observed comparing equations (4.10) and (4.15). To evade this inconsistency, initial conditions are taken with $A_0/2$ instead of A_0. As shown in the figure 4.1 and figure 4.2, the results are similar. Observed oscillations may be attributed to the competition between self-focusing and plasma defocusing.

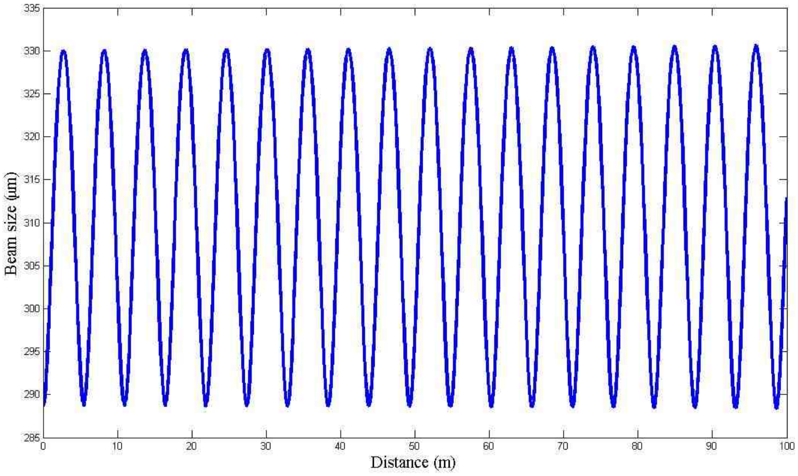

Figure 4.2: Evolution of the gaussian beam, with $A_0 = 1, \omega_0 = 1/\sqrt{0.12}$.

4.1.2 Ring Trial Function.

The variational approach is also applicable for the derivation of vortex beam waist evolution equations. The Lagrangian $\mathcal{L}$ corresponding to the equation with cubic-quartic nonlinearity includes azimuthal variable

$$\mathcal{L} = \frac{i}{2}(\psi^* \frac{\partial \psi}{\partial z} - \psi \frac{\partial \psi^*}{\partial z}) - \left| \frac{\partial \psi}{\partial r} \right|^2 - \frac{1}{r^2} \left| \frac{\partial \psi}{\partial \theta} \right|^2 + \frac{1}{2} |\psi|^4 - \frac{2}{5} |\psi|^5. \tag{4.16}$$

A suitable trial function corresponding to the vortex beam problem has the following form

$$\psi(r, z) = A(z) r^m e^{-\left(\frac{r^2}{a^2(z)} + iC(z) r^2 + im\theta + i\phi(z) \right)}. \tag{4.17}$$

After averaging, the reduced Lagrangian can be expressed for any charge m

$$< \mathcal{L} >= \alpha_1 A^2 \phi' + \alpha_2 A^2 (C' - 4C^2) - \alpha_3 A^2 - \alpha_4 A^2 + \alpha_5 A^4 - \alpha_6 A^5 \tag{4.18}$$

where $\alpha_i = \alpha_i(a)$ is listed below

$$\begin{aligned}
\alpha_1 &= \int_0^\infty e^{-\frac{2r^2}{a^2}} r^{2m+1} dr \\
\alpha_2 &= \int_0^\infty e^{-\frac{2r^2}{a^2}} r^{2m+3} dr \\
\alpha_3 &= \int_0^\infty e^{-\frac{2r^2}{a^2}} r^{2m+1} \left(\frac{m}{r} - \frac{2r}{a} \right)^2 dr \\
\alpha_4 &= m^2 \int_0^\infty e^{-\frac{2r^2}{a^2}} r^{2m-1} dr
\end{aligned}$$

$$\alpha_5 = \frac{1}{2}\int_0^\infty e^{-\frac{4r^2}{a^2}} r^{4m+1} dr$$
$$\alpha_6 = \frac{2}{5}\int_0^\infty e^{-\frac{5r^2}{a^2}} r^{5m+1} dr.$$

After taking variations and using the Euler-Lagrange equations, evolution equations are obtained for any m, for example

for $m = 1$:

$$\frac{d^2a}{dz^2} = \frac{64 - A_0^2 a_0^2}{4a^3} + \frac{18}{625}\frac{A_0^3 a_0^3 \mu\sqrt{5\pi}}{a^4} \tag{4.19}$$

for $m = 2$:

$$\frac{d^2a}{dz^2} = \frac{128 - A_0^2 a_0^2}{8a^3} + \frac{768}{15625}\frac{A_0^3 a_0^3 \mu}{a^4}. \tag{4.20}$$

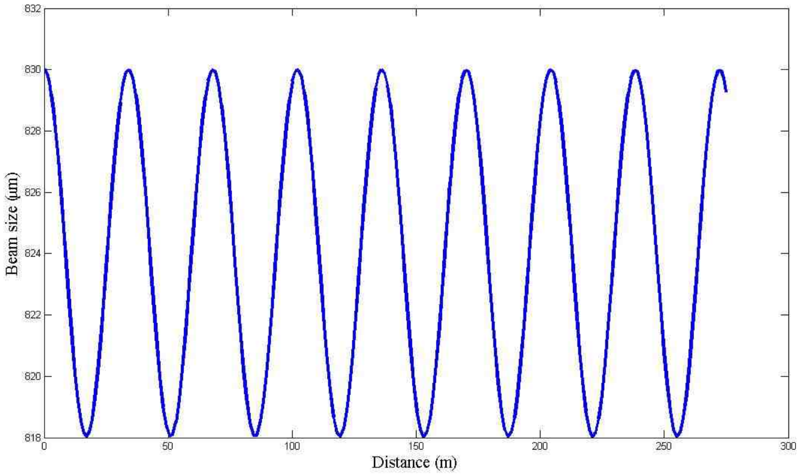

Figure 4.3: Beam width propagation of vortex $A_0 r e^{-r^2/a_0^2}$.

Initial conditions $A_0 = 1.66, a_0 = 7.9$ correspond to the fit of the stationary solution obtained at $\Lambda = 0.12$. The dynamics of the vortex beam waist parameter on the figure 4.3 shows periodic oscillations over hundreds of meters and increasing oscillations after 600 meters, followed be infinite increase at around 1000. The cause of this may be azimuthal instability.

4.2 Stability of stationary solutions.

Several methods of stability analysis that were developed in the nonlinear waves theory can be applied to stationary localized solutions obtained in Chapter 3. Discussions of different techniques are given by these authors [48, 49, 50, 51, 52, 53, 54, 55].

For equations of the Hamiltonian type, the variational method is usually the standard approach. In this formulation, ground state solutions are stationary points of the Hamiltonian H at fixed functional $N = \int |\psi|^2$, which usually defines a beam power. Stability follows if it can be shown that the bound state produces a minimum of H. The absence of minimizers does not imply the instability of the states. This analysis is sometimes called nonlinear because it doesn't use the linearization technique. This method is applied to the stationary problem with cubic-quartic nonlinearity.

Another approach tackles the question of linear stability with respect to small perturbations. In this case, stability of the stationary solution is assumed local in contrast to absolute extremum of the Hamiltonian. This technique uses the linearization of the equations on the background of ground state solution to study the spectrum of differential operators.

Since dimensionality of the stationary solution is less than the dimensionality of the initial problem, linear stability is divided into two parts. In the first part, stability is examined with respect to small perturbations of the same dimensionality. In the second part of analysis, stability of the stationary continuous wave is checked against spatiotemporal perturbations.

4.2.1 Nonlinear stability.

Analysis starts with defining the Hamiltonian for cubic-quartic nonlinearity

$$H = \int |\triangle_\perp \psi|^2 - \frac{1}{2}|\psi|^4 + \frac{2}{5}|\psi|^5 dxdy.$$

Following [33], assume that $\psi_s(x, y)$ is the solution of

$$-\Lambda\psi + \nabla_\perp^2\psi + |\psi|^2\psi - |\psi|^3\psi = 0.$$

Now, let's apply a transformation that preserves the power N

$$\tilde{\psi}(\tilde{x}, \tilde{y}) = \frac{1}{a}\psi\left(\frac{x}{a}, \frac{y}{a}\right).$$

After substitution, the Hamiltonian has the following form

$$H(a) = \frac{1}{a^2}\int |\triangle_\perp \psi|^2 dxdy - \frac{1}{2}\frac{1}{a^2}\int |\psi|^4 dxdy + \frac{2}{5}\frac{1}{a^3}\int |\psi|^5 dxdy.$$

Since the ground state is a solution of the following variational problem $\delta\{H + \lambda^2 N\} = 0$ and N is preserved with varying a, it follows

$$\frac{\partial H}{\partial a} = -\frac{2}{a^3}M_1 + \frac{1}{a^3}M_2 - \frac{6}{5}\frac{1}{a^4}M_3 = 0$$

under the constraint $a = 1$. Here, $M_1 = \int |\triangle_\perp \psi|^2 dxdy$, $M_2 = \int |\psi|^4 dxdy$, $M_3 =$

$\int |\psi|^5 dxdy$ and one can observe that all these quantities are positive, hence

$$M_2 = 2M_1 + \frac{6}{5}M_3.$$

Stability can be determined from the sign of the second derivative of the Hamiltonian

$$\frac{\partial^2 H}{\partial a^2} = 6M_1 - 3M_2 + \frac{24}{5}M_3 = \frac{6}{5}M_3 > 0.$$

This means that the ground state ψ_s is a minimum of $H(a)$ and it is stable.

4.2.2 Spatial perturbations.

In the previous section, stability was addressed by means of the variational approach. However this method is not suitable for the equation (3.5) with $F_1(|\psi|^2)$ nonlinearity. In this case stability is investigated with respect to small spatial perturbations.

Consider the stationary localized solution obtained in chapter 3, $\psi(x, y, z) = \psi_s(x, y)e^{i\Lambda z}$. Let's perturb it and expand, keeping only the first order correction

$$\psi(x, y, z) \approx (\psi_s(x, y) + u(x, y, z) + iv(x, y, z))e^{i\Lambda z} \tag{4.21}$$

where $u(x, y, z), v(x, y, z)$ are real functions. After substitution to the equation (3.4), u, v satisfy the system

$$\partial_z \begin{pmatrix} u \\ v \end{pmatrix} = N \begin{pmatrix} u \\ v \end{pmatrix}$$

where

$$N = \begin{pmatrix} 0 & L_0 \\ -L_1 & 0 \end{pmatrix}$$

and

$$L_0 = -\triangle_\perp + \Lambda - \psi_s^2 - \mu + \sqrt{\mu^2 + \psi_s^6}$$
$$L_1 = -\triangle_\perp + \Lambda - 3\psi_s^2 - \mu + \sqrt{\mu^2 + \psi_s^6} + \frac{6\psi_s^6}{\sqrt{\mu^2 + \psi_s^6}}$$

are self-adjoint operators. If perturbations u, v are defined as $fe^{\imath\kappa z}$ and $ge^{\imath\kappa z}$, the system can be reduced to a single equation of the form

$$\kappa^2 f = L_0 L_1 f \tag{4.22}$$

The goal of this analysis is to determine the sign of κ^2. If it can be shown that $\kappa^2 > 0$ for all bounded states, then (neutral) stability implies, otherwise the equilibrium solution is unstable.

Let's define operator $G_0 = -\triangle_\perp + \Lambda - \psi_s^2$. Then one can check that

$$G_0 = -\frac{1}{\psi_s} \bigtriangledown \cdot \left(\psi_s^2 \bigtriangledown (\frac{1}{\psi_s} \cdot) \right)$$

hence

$$\int f L_0 f dxdy = \int \left| \bigtriangledown \left(\frac{f}{\psi_s} \right) \right|^2 \psi_s^2 dxdy + \int (-\mu + \sqrt{\mu^2 + \psi_s^6}) f^2 dxdy \geq 0$$

which means that the operator L_0 is nonnegative, and it follows that for a solution

f, the minimum value of κ^2 is given by

$$\kappa_m^2 = \min \frac{< f|L_1|f >}{< f|L_0^{-1}|f >}$$

where $< f|L|f >= \int fLfrdr$. The sign of κ_m^2 is then determined by the numerator $\mu_{min} =< fL_1 f >$. This in turn comes down to the spectral problem for L_1, i.e.

$$L_1 f = \sigma f + \rho \psi_s \tag{4.23}$$

where σ and ρ are chosen to satisfy $< f|f >= 1$ and $< f|\psi_s >= 0$. Notice that if equation (4.34) is multiplied by f from the left then the sign of μ_{min} will be negative depending on whether there is a solution of the spectral problem with $\sigma < 0$.

Functions f and ψ_s can be expanded in terms of orthogonal eigenfunctions ψ_n of the operator L_1 ($L_1\psi_n = \lambda_n \psi_n$). These series are substituted in equation (4.34) to obtain

$$f = \rho \sum \frac{< \psi_s|\psi_n >}{\lambda_n - \sigma}. \tag{4.24}$$

Equation (4.35) and the orthogonality constraint produces the following relation

$$S(\sigma) = \rho \sum \frac{< \psi_s|\psi_n >< \psi_n|\psi_s >}{\lambda_n - \sigma}. \tag{4.25}$$

The sum does not contain zero eigenvalue and it has been proven [49] that operator L_1 has only one negative eigenvalue. Hence when σ changes from negative to positive eigenvalue, the function $S(\sigma)$ changes from $-\infty$ to $+\infty$ passing zero. Therefore the sign of σ_{min} is determined by the sign of $S(0)$. Since $S(\sigma)$ is a monotonically increasing function then $S(0) < 0$ means that $S(\sigma) = 0$ at some $\sigma > 0$ and vice versa.

It follows from equations (4.35) and (4.36) that $S(0) =< \psi_s|L_1^{-1}|\psi_s >$. In order to find $S(0)$, the expression $L_0\psi_s = 0$ is differentiated with respect to Λ. The resulting equation is written in the following form

$$L_1 \frac{\partial \psi_s}{\partial \Lambda} = -\psi_s.$$

Taking the inverse of L_1 and multiplying both sides from the left by ψ_s the following equation is obtained

$$S(0) = -\frac{1}{2}\frac{\partial P}{\partial \Lambda}$$

where $P = \int \psi_s^2 dxdy$.

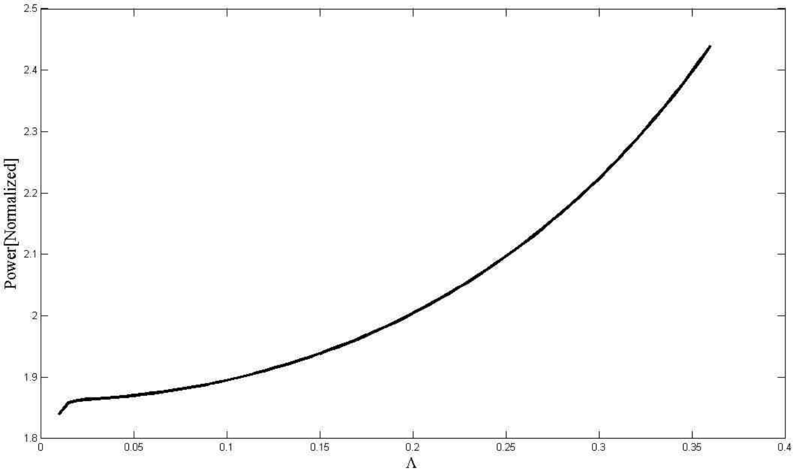

Figure 4.4: Power of the steady state solution vs eigenvalues Λ.

The Vakhitov-Kolokolov criterion [48] states that the equilibrium solution is stable whenever $dP/d\Lambda > 0$ and unstable otherwise. As shown in figure 4.4, the power is an increasing function of Λ, meaning that stability criterion is satisfied at least for the range of the given values of Λ. If perturbations are only radial, the Vakhitov-Kolokolov criterion can also be applied to the stationary vortex solutions. Figure 4.5 shows that localized vortices with different indices m are stable against such perturbations. This analysis however is not enough as ring-shaped solutions may suffer from modulational instability in the azimuthal direction. The next section is devoted to such problems.

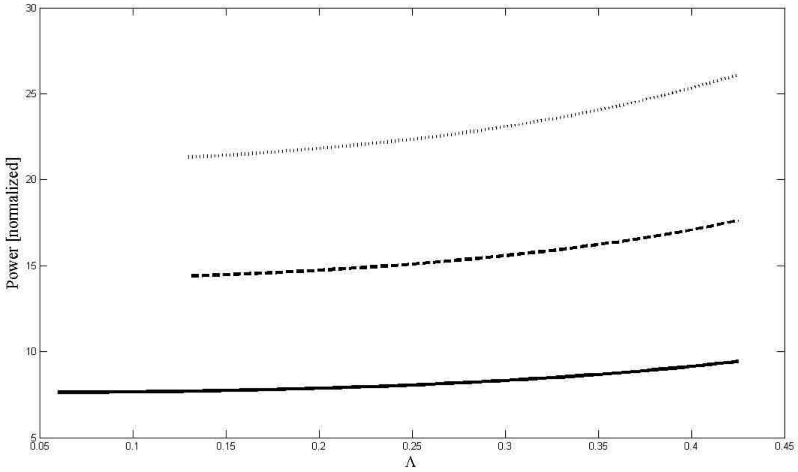

Figure 4.5: Power of the steady state vortex solutions for m=1,2,3 vs eigenvalues Λ.

4.2.3 Azimuthal perturbations.

Azimuthal instability of optical vortices has been studied numerically in different nonlinear media. It tends to split up the vortex into the set of fundamental solutions, causing the symmetry to break. This was later shown experimentally [56].

The purpose of this section is to formulate and study the spectral problem that emerges in the presence of the azimuthal perturbations. To begin, let's perturb the amplitude of the stationary solution $\psi(r)$ by a function of the integer azimuthal index L. Perturbations will be applied along the radius r_m, which is defined as $r_m^2 = \int r^2 |\psi_m|^2 dr / P_m$, where P_m is the power of the vortex

$$\psi(z, \theta) = \left(\psi_s + a_+ e^{-i(L\theta + \lambda z)} + a_- e^{i(L\theta + \bar{\lambda} z)}\right) e^{i\Lambda z + im\theta}. \tag{4.26}$$

Here, ψ_s is assumed to be a constant intensity defined as $\psi_s = \psi_s(r = r_m)$ for some fixed m. It can be seen from the setup that solution is unstable if λ has a nonzero imaginary part and is stable otherwise. To find the instability growth rate, ansatz (4.26) is plugged into the propagation equation (3.5). Two coupled equations are obtained after linearization with respect to the perturbations

$$i(\Lambda - \lambda) a_+ = -i \frac{(m - L)^2}{r_m^2} a_+ + iBa_+ + iC\bar{a}_- \tag{4.27}$$

$$i(\Lambda + \bar{\lambda}) a_- = -i \frac{(m + L)^2}{r_m^2} a_- + iBa_- + iC\bar{a}_+ \tag{4.28}$$

where for $F_1(|\psi|^2)$:

$$B = 2\psi_s^2 - (-\mu + \sqrt{\mu^2 + \psi_s^6}) - \tfrac{3}{2} \tfrac{\psi_s^6}{\sqrt{\mu^2 + \psi_s^6}}, \qquad C = \psi_s^2 - \tfrac{3}{2} \tfrac{\psi_s^6}{\sqrt{\mu^2 + \psi_s^6}}$$

and for $F_2(|\psi|^2)$:

$$B = 2\psi_s^2 - \tfrac{5}{2}\psi_s^3, \qquad C = \psi_s^2 - \tfrac{3}{2}\psi_s^3.$$

The above equations can be rewritten in the matrix form

$$i\begin{pmatrix} \Lambda-\lambda & 0 \\ 0 & -\Lambda-\lambda \end{pmatrix}\begin{pmatrix} a_+ \\ \bar{a}_- \end{pmatrix} = i\begin{pmatrix} -\frac{(L-m)^2}{r_m^2}+B & C \\ -C & \frac{(L+m)^2}{r_m^2}-B \end{pmatrix}\begin{pmatrix} a_+ \\ \bar{a}_-. \end{pmatrix}$$

The determinant is equated to zero to obtain

$$\lambda = -\frac{2Lm}{r_m^2} \pm \sqrt{\left(\frac{(L^2+m^2)}{r_m^2}+\Lambda-B\right)^2 - C^2}. \tag{4.29}$$

To look for the growth rate, we need to look at the imaginary part of Λ

$$\mathrm{Im}\,(\lambda) = \mathrm{Im}\sqrt{\left(\frac{(L^2+m^2)}{r_m^2}+\Lambda-B\right)^2 - C^2}. \tag{4.30}$$

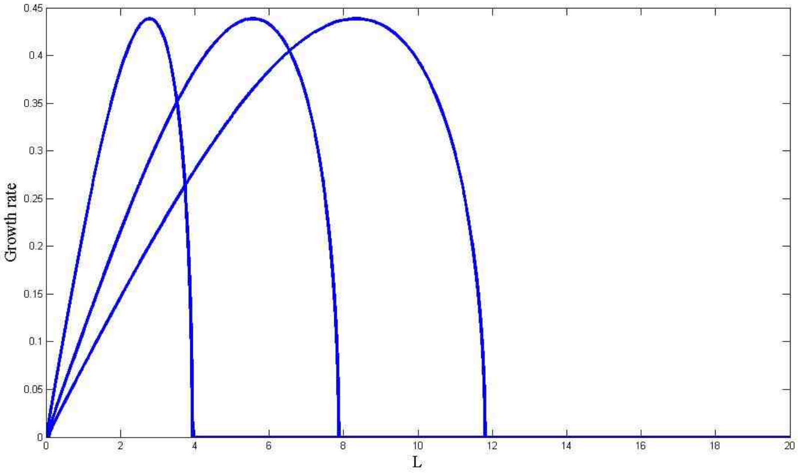

Figure 4.6: Growth rate of the stationary vortices as a function of the azimuthal index L for different values of m=1,2,3

Figure 4.6 shows the instability growth rate for different charges m. Although the index L is represented as a real parameter, it must be an integer in order to preserve azimuthal periodicity. The maximum growth rate for $m = 1$ is approximately attained at $L = 3$ and for $m = 2$ is at $L = 5$. Instability is bounded by larger number L and the maximum growth rate is approximately at the same level for any m.

4.2.4 Spatiotemporal perturbations.

In order to investigate the time-perturbed solution, the plasma equation needs to be nondimensionalized. It is done with the following transformation

$$N_e \to N_{e_0} N_e, \quad t \to t_0 t.$$

The nondimensional equations are given

$$i\psi_z + \nabla_\perp^2 \psi + |\psi|^2 \psi - N_e(\psi)\psi = 0 \tag{4.31}$$

$$\frac{\partial N_e}{\partial t} = |\psi|^6 - N_e^2 - \nu N_e \tag{4.32}$$

where the additional normalization constants are defined in the following way

$$N_{e_0} = \sqrt{\frac{\sigma N_0 n_0^3}{8\eta^3 \beta_{ep}} \mathcal{E}_0^3}, \quad t_0 = \frac{1}{\beta_{ep} N_{e_0}}, \quad \nu = \gamma t_0$$

Lets introduce the perturbation fields

$$\psi(z, r, t) = (\psi_s(r) + u(z, r, t) + iv(z, r, t))e^{i\Lambda z + im\theta} \tag{4.33}$$

$$N_e(z, r, t) = N_{e_s}(r) + \delta N_e(z, r, t) \tag{4.34}$$

where $u, v, \delta Ne \propto \exp(-i\Omega t + i\kappa z)$.

The main principle of this approach is to study the spectrum of the wave modes along t-direction that are slightly different from the neutrally stable one (when $\Omega = 0$ and $\kappa = 0$). This method was developed by Kuznetsov et al [51].

By putting the perturbed modes (4.43),(4.44) into equation (4.42) and using simple algebra, the result is

$$\delta N_e = \frac{6\psi_s^5 u}{2N_{e_s} + \nu - i\Omega} \tag{4.35}$$

Substituting (4.43),(4.44) into (4.41), along with (4.45) and linearizing against the background of a stationary solution, the coupled equations for perturbation fields are obtained. They can be reduced to two independent equations

$$L_0(L_1 + \delta L)u = \kappa^2 u \tag{4.36}$$

$$(L_1 + \delta L)L_0 v = \kappa^2 v \tag{4.37}$$

where L_0 and L_1 are operators from the section 4.3.2, and

$$\delta L = \frac{6\psi_s^6}{\sqrt{\mu^2 + \psi_s^6} - i\Omega} - \frac{6\psi_s^6}{\sqrt{\mu^2 + \psi_s^6}}. \tag{4.38}$$

In the case $\Omega = 0$, it is clear that $\delta L = 0$ and equation (4.46-4.47) can be examined through Vakhitov-Kolokolov criterion. If $\Omega \neq 0$, the spectrum of the given spectral problem can be defined using perturbation expansion with neutrally stable modes as the first approximation. By multiplying (4.48) from the left by $r\psi_s$ and assuming $v_0 = r\psi_s$, it follows

$$\kappa^2 =< \psi_s \psi_{sr} | \delta L | \psi_s \psi_{sr} > . \tag{4.39}$$

The applicability criterion of this formula is the condition $\kappa << \Lambda$. Although instability is present for any $\Omega \neq 0$, it follows directly from the setup of the equations (4.46-4.47) that $\kappa^2 > 0$ if $\Omega \rightarrow \infty$. Hence the growth rate decreases as $\Omega \rightarrow \infty$ and the maximum growth rate is determined by the equation (4.50). While it is challenging to find an exact maximum, it is shown in figure 4.7 that the growth rate is limited.

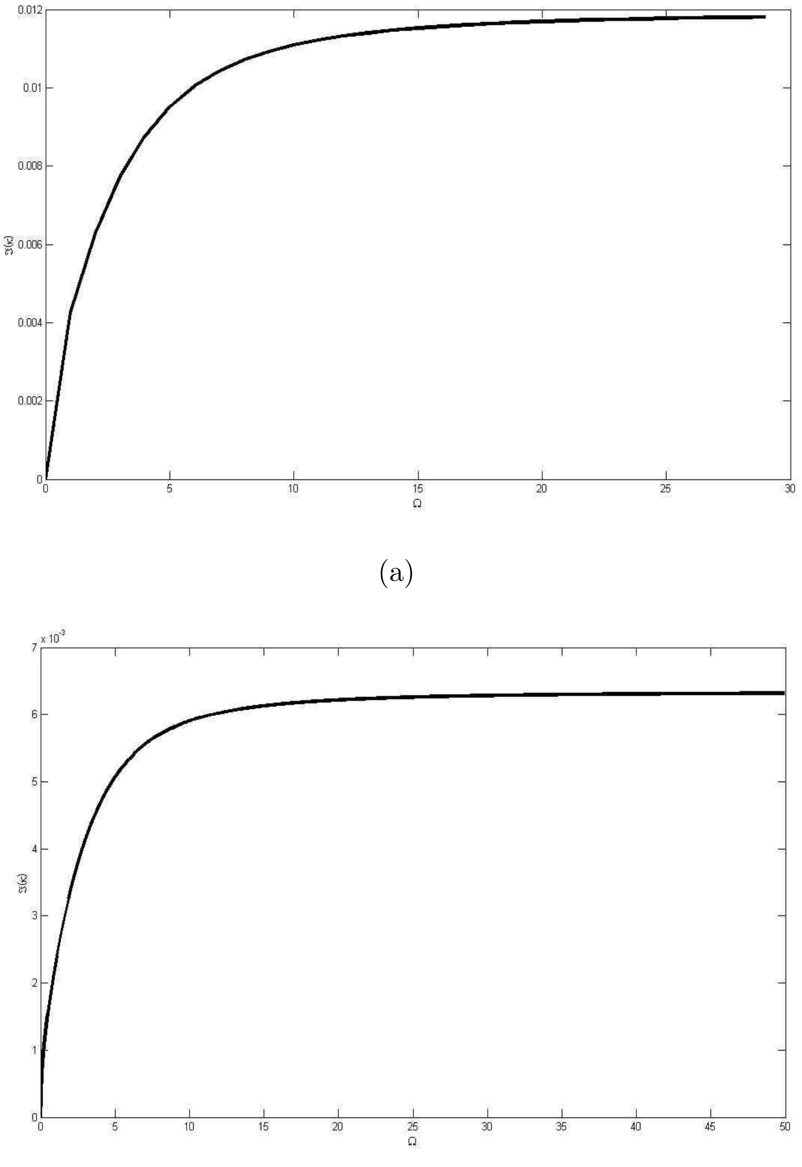

(a)

(b)

Figure 4.7: Growth rate vs Ω (a) fundamental solution at Λ=0.205, (b) m=1 vortex solution at Λ=0.165

Chapter 5

Numerical simulations

This chapter provides numerical results using non-dimensional propagation models. In the first section the $(2+1)D$ stationary model is integrated numerically. In this case it is assumed that the pulse is long enough to be considered as a continuous wave. In the second section, the beam is confined in time in order to produce a finite pulse. Therefore the time dimension is included and the dynamics of the non-stationary profiles are investigated in the more realistic $(3+1)D$ problem. Last section presents propagation of the pulse perturbed by random noise in the model with included nonlinear losses. In all scenarios, propagation of the pulse is provided by the Fourier split-step method which is detailed in Appendix A. The propagation code was written in C and used the MPI library. The simulations were made on a linux cluster (NANO) from the Center for Advanced Research Computing at the University of New Mexico, which computational power expands up to 144 CPUs. The results of the simulations were plotted using Matlab graphing utilities.

5.1 (2+1)D simulations.

To confirm theoretical results obtained in the previous chapter direct numerical simulations are performed using stationary model

$$i\frac{\partial\psi}{\partial z} + \nabla_{\perp}^{2}\psi + |\psi|^{2}\psi - F(|\psi|^{2})\psi = 0 \tag{5.1}$$

where $\psi = \psi(x, y, z)$. The split-step method uses linear and nonlinear operators which are defined

$$L(\psi) = \nabla_{\perp}^{2}\psi, \quad N(\psi) = |\psi|^{2} - F(|\psi|^{2}) \tag{5.2}$$

In the first numerical simulation, the initial condition is chosen to be the gaussian of the following form

$$\psi(x, y, 0) = A_0 e^{-(x^2+y^2)/\omega_0^2} \tag{5.3}$$

where the values of amplitude A_0 and beam width w_0 were found in chapter 3 to fit the stationary solution at $\Lambda = 0.205$. Figure (5.1) shows the distribution of the electric field for different propagation distances along 100 meters for model with $F_1(|\psi|^2)$ nonlinearity. Observed small oscillations conform to the prediction by the semi-analytical approach. Due to the excess of power and inability to match the exact steady state solution, the gaussian profile is responsible for a small outflow of radiation during propagation.

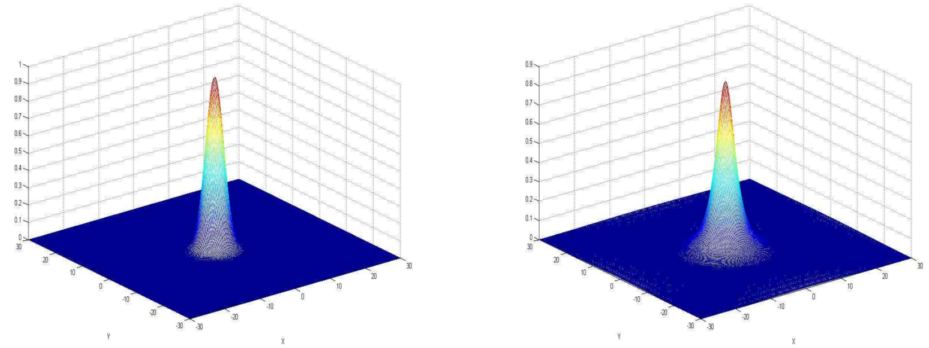

(a) z=0 m (b) z=10.75 m

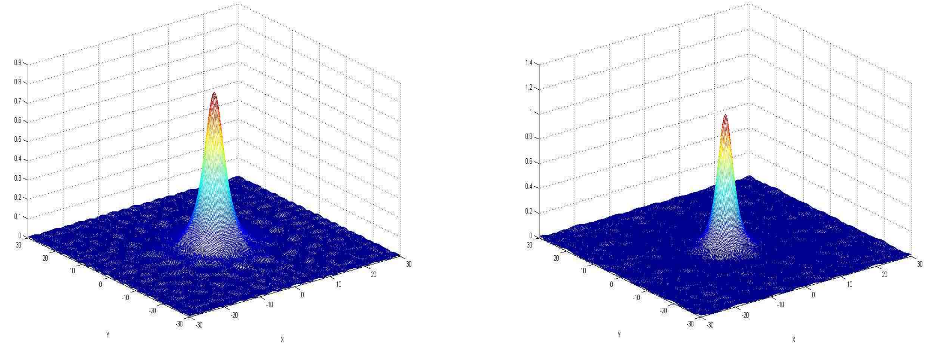

(c) z=32.27 m (d) z=53.78 m

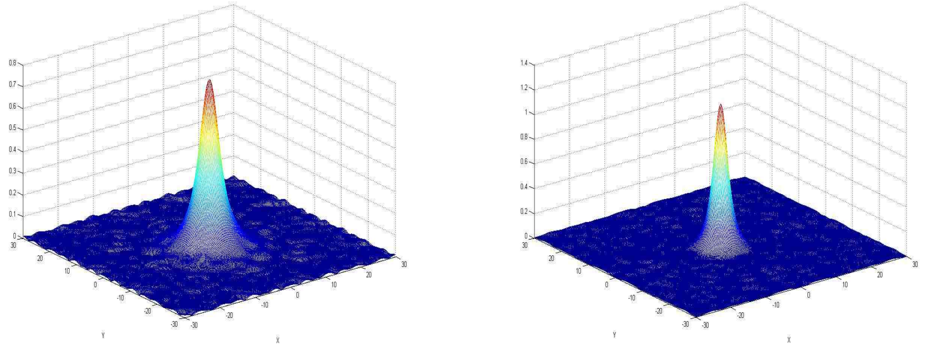

(e) z=75.3 m (f) z=96.8 m

Figure 5.1: Propagation of gaussian beam $A_0 e^{-(x^2+y^2)/\omega_0^2}$ with $A_0 = 1, \omega_0 = 1/\sqrt{0.12}$.

The second simulation presents propagation of the ring-shaped beams with the following initial shape

$$\psi(x, y, 0) = A_m (r/w_0)^m e^{-r^2/2\bar{r}_m^2 + im\theta}. \tag{5.4}$$

The azimuthal angle of this input is perturbed at the peak amplitude by azimuthal index L that corresponds to the growth rate maximum. Figures (5.2) – (5.5) show the results of the simulations. During propagation, the ring-shaped beam loses power via small outgoing radiation waves and fits the steady state keeping its shape over several meters. The azimuthal instability starts to make impact around 10 meters and eventually breaks up the ring into a number of moving fundamental solutions that move away from each other. This number corresponds to azimuthal index L which is in excellent agreement with predictions from chapter 4.

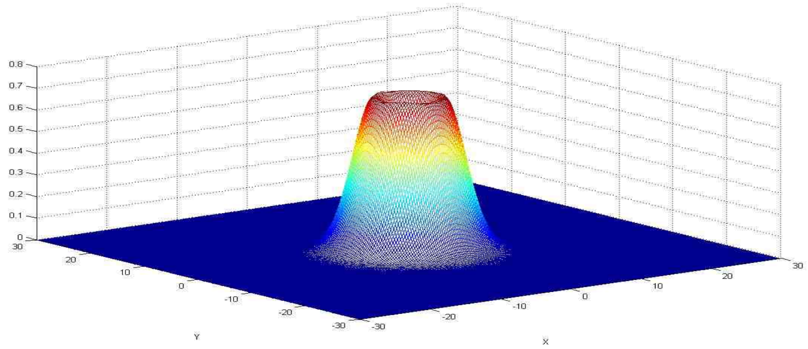

(a) z=0 m

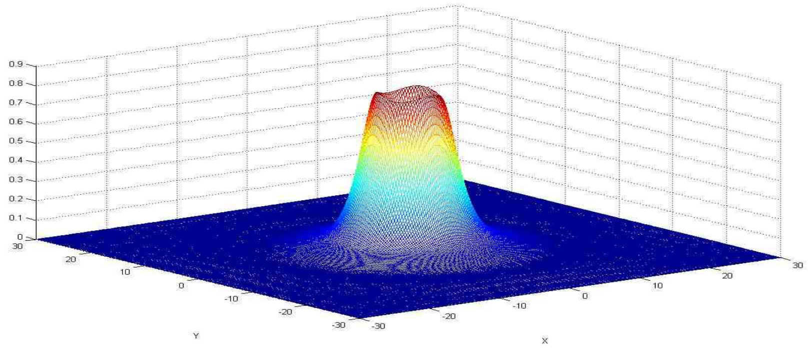

(b) z=10.76 m

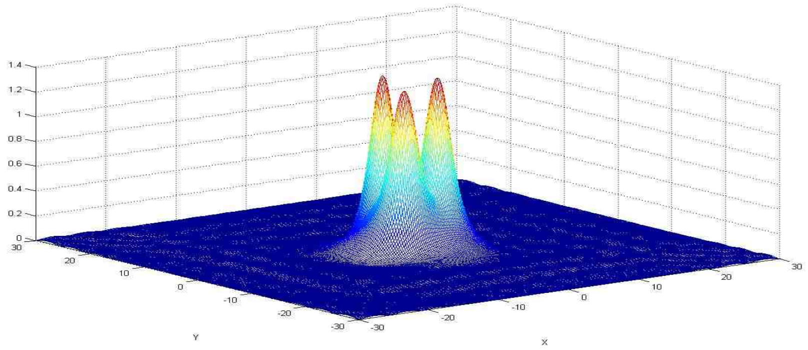

(c) z=21.5 m

Figure 5.2: Vortex propagation m=1, $L = 3$

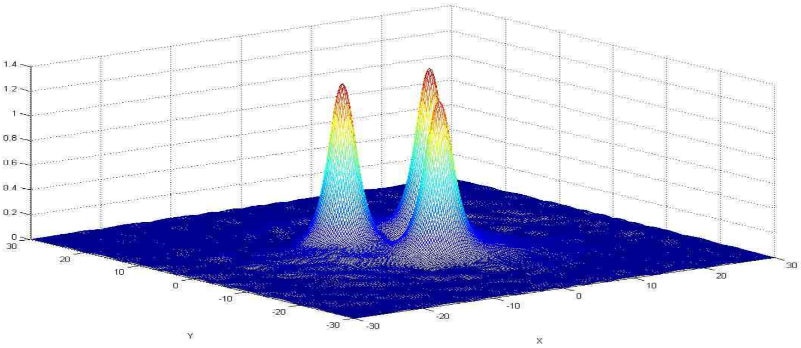

(a) z=32.26 m

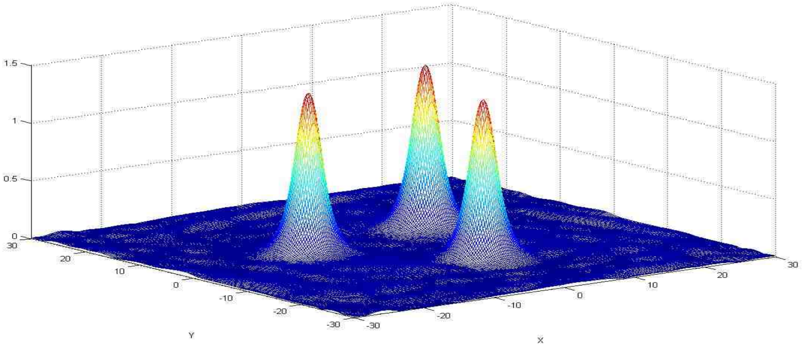

(b) z=43.03 m

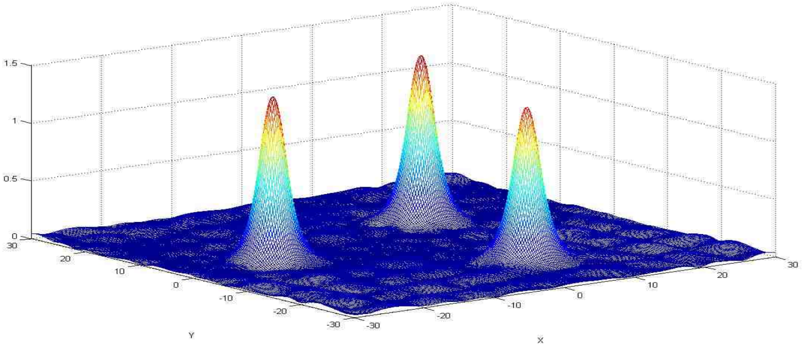

(c) z=53.78 m

Figure 5.3: Vortex propagation $m = 1$, $L = 3$

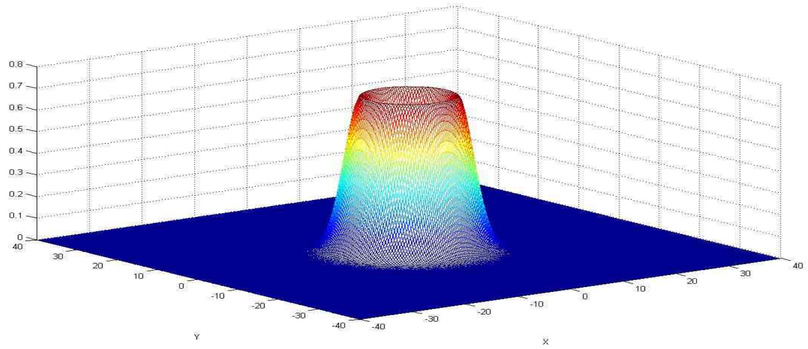

(a) z=0 m

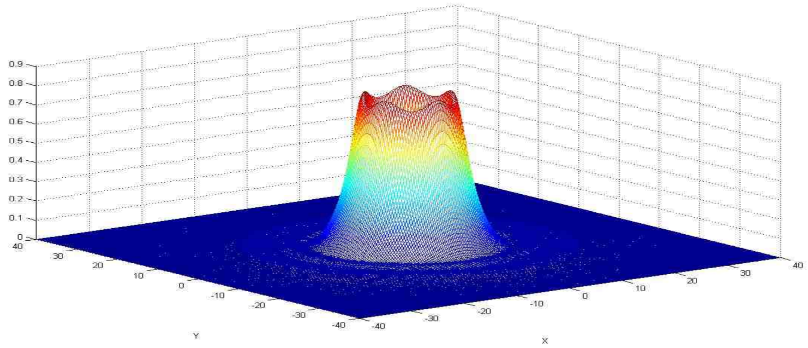

(b) z=9.84 m

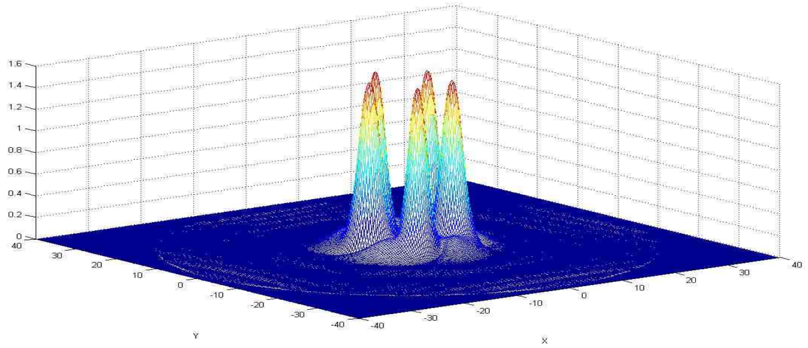

(c) z=19.68 m

Figure 5.4: Vortex propagation $m = 2$, $L = 5$

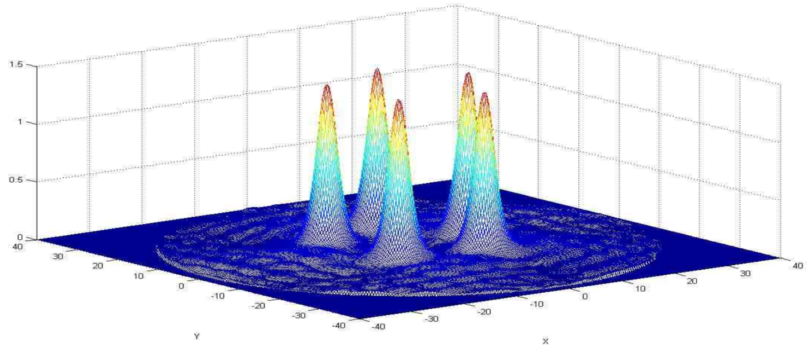

(a) z=39.37 m

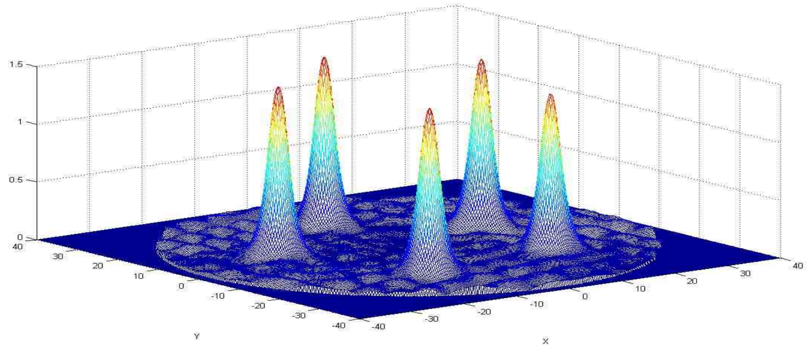

(b) z=59.05 m

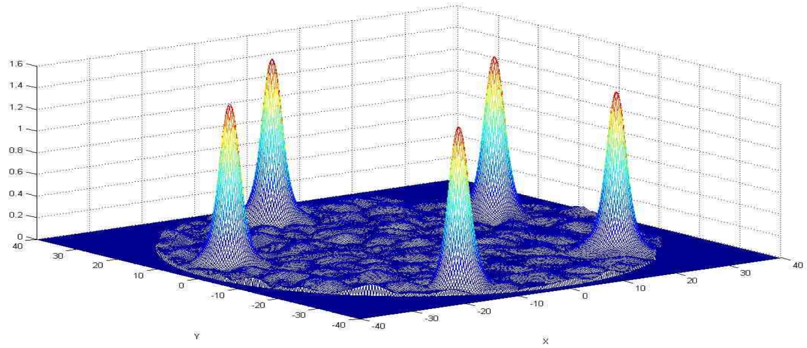

(c) z=78.74 m

Figure 5.5: Vortex propagation $m = 2$, $L = 5$

5.2 (3+1)D simulations.

The equations of the (3+1)D model are given

$$i\psi_z + \nabla_\perp^2\psi + |\psi|^2\psi - N_e(\psi)\psi = 0 \tag{5.5}$$

$$\frac{\partial N_e}{\partial t} = |\psi|^6 - N_e^2 - \nu N_e \tag{5.6}$$

where $\psi = \psi(x, y, z, t)$ and $N_e = N_e(x, y, z, t)$.

Integration starts with the assumption that no plasma is present at the position $z = 0$. After evaluation of the electric field at the next propagation step, plasma density is numerically computed from the equation (5.6) using the fourth-order RungeKutta method

$$\begin{aligned}
&N_{e_{n+1}} = N_{e_n} + \frac{1}{6}\left(K_1 + 2K_2 + 2K_3 + K_4\right)\\
&t_{n+1} = t_n + \Delta t,\\
&K_1 = \Delta t f(t_n, N_{e_n}),\\
&K_2 = \Delta t f\left(t_n + \frac{1}{2}\Delta t, N_{e_n} + \frac{1}{2}K_1\right),\\
&K_3 = \Delta t f\left(t_n + \frac{1}{2}\Delta t, N_{e_n} + \frac{1}{2}K_2\right),\\
&K_4 = \Delta t f(t_n + \Delta t, N_{e_n} + K_3),
\end{aligned}$$

where $f(t_n, N_{e_n}) = |\psi(z_m, t_n)|^6 - N_{en}^2 - \nu N_{en}$, $z_m = m\Delta z$.

To create a nanosecond pulse the following initial conditions are used

$$\psi(x, y, 0, t) = \psi(x, y, 0)e^{-t^2/t_p^2} \tag{5.7}$$

where $\psi(x, y, 0)$ is the 2D initial condition from previous section.

The results of the simulations are shown on Figures (5.6) $-$ (5.9). Dynamics of the nanosecond pulse differ from the small oscillations around equilibrium of the stationary model predicted by the theory. Propagation develops into the collapse event, as a pulse of a finite temporal duration is not exact steady state. Exact distance at which regularization of the collapse is attained is unknown due to the inability to capture further increase of the amplitude with the current uniform grid.

5.3 Numerical tests and convergence.

To check the validity of the results, several tests were employed. First, it was observed that the power and the energy of the pulse stay conserved during propagation within 0.01% of accuracy. In (2+1)D model, the tests were done at the distances where the radiation outflow is negligible. The loss of power further is attributed to the absorbtion of the radiation waves on the boundaries, by removing corresponding frequencies in the Fourier domain.

To verify the error convergence, simulations were done for different values of h and Δt. Number of points in the computational grids were chosen among $128, 256, 512$ in each direction. When h was divided by two, Δz was divided by four, in order to eliminate the growth of the numerical instability.

Another test checks the convergence of the plasma density to the steady state solution in the equation (5.6) for various values of Δt. Finally, initial condition (5.3) was used in the (3+1)D model in order to check the stability of the stationary solution under the current numerical scheme. It was observed that the growth of the numerical errors eventually destroys stability for large values of z.

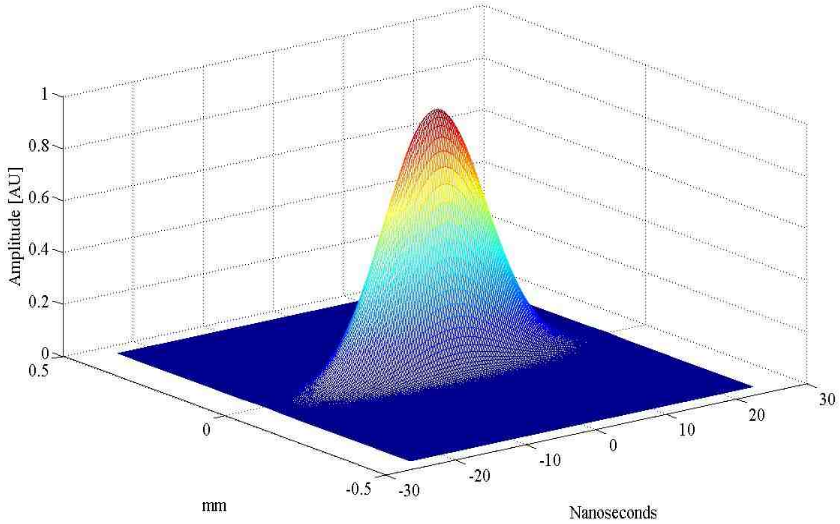

(a) Pulse at z=0 m

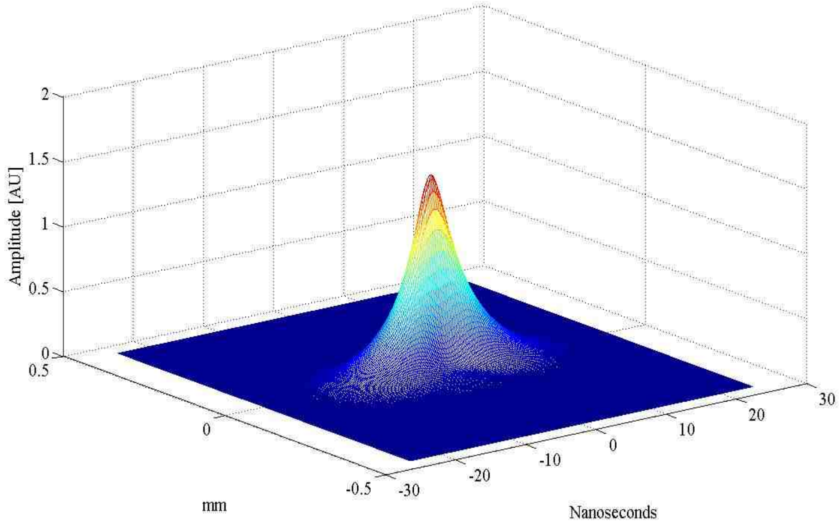

(b) Pulse at z=3.5 m

Figure 5.6: Propagation of 10 nanosecond pulse

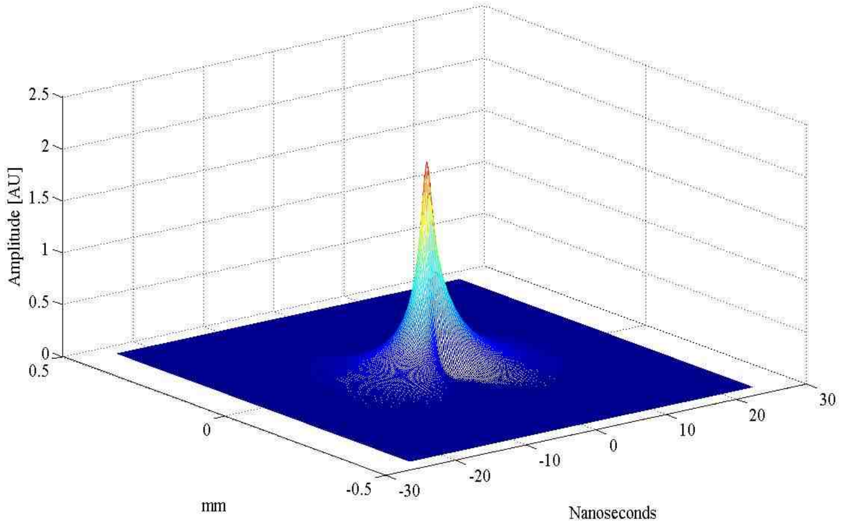

(a) Pulse at z=7.5 m

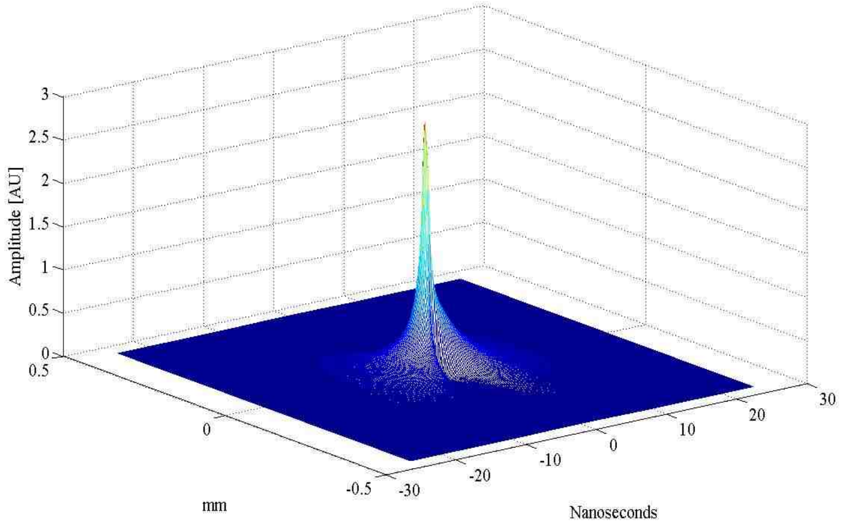

(b) Pulse at z=10 m

Figure 5.7: Propagation of 10 nanosecond pulse

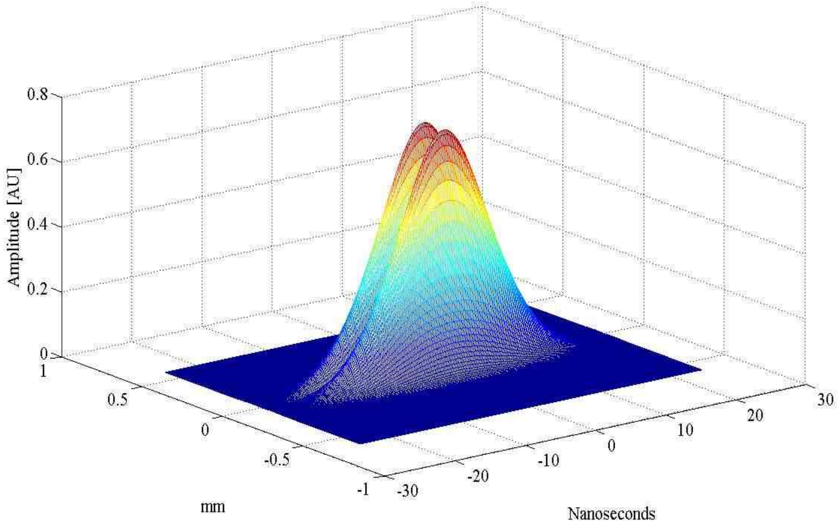

(a) z=0 m

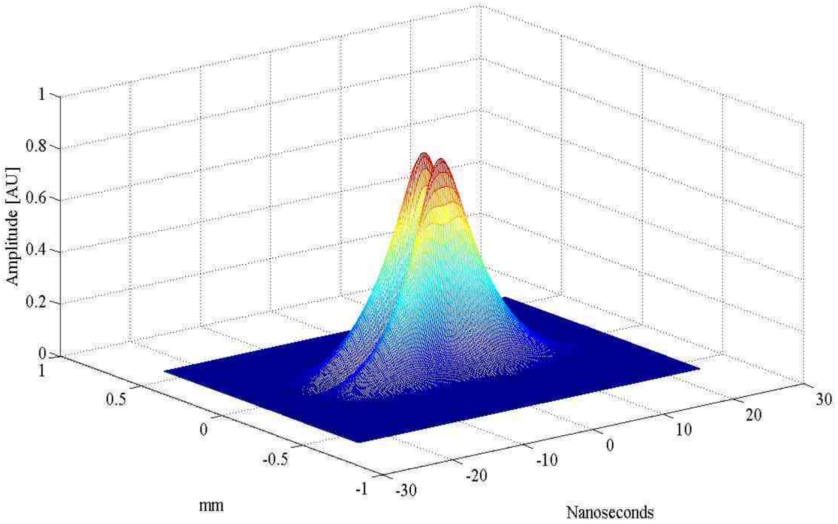

(b) z=9 m

Figure 5.8: Propagation of 10 nanosecond m=1 vortex pulse

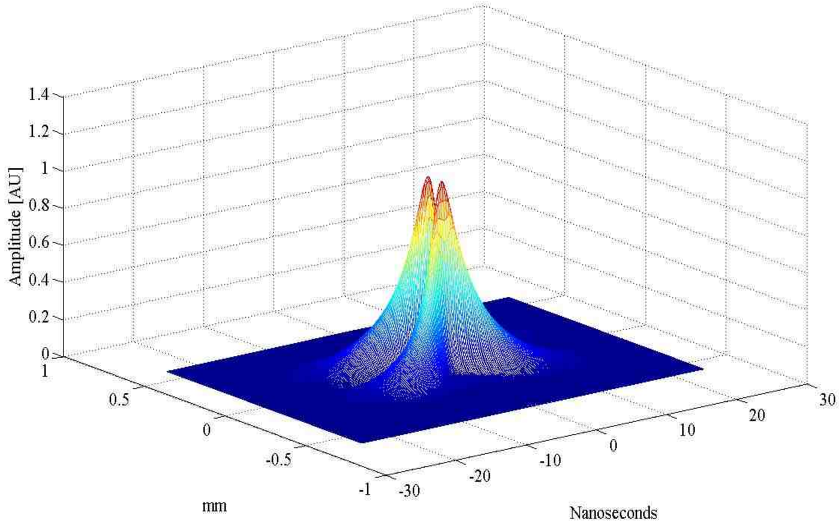

(a) z=16.5 m

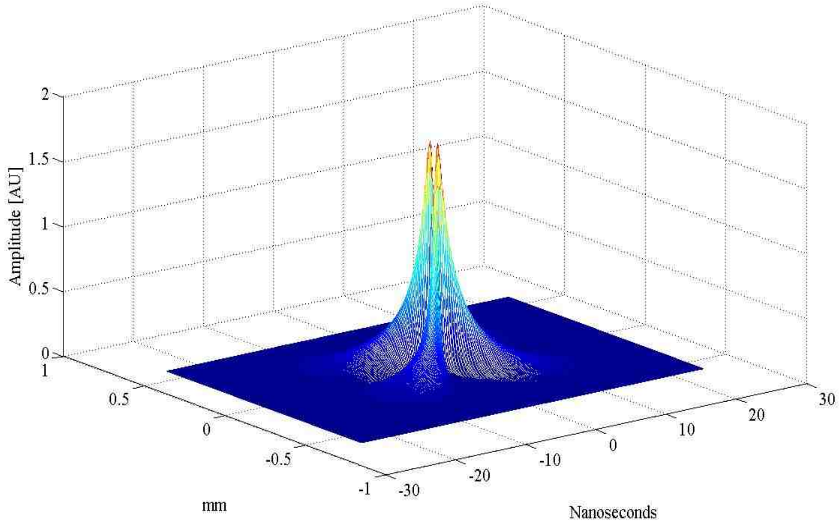

(b) z=22 m

Figure 5.9: Propagation of 10 nanosecond m=1 vortex pulse.

5.4 (3+1)D model with nonlinear losses.

In the final simulation, the equation (5.5) is considered with the nonlinear losses

$$i\psi_z + \nabla_\perp^2 \psi + |\psi|^2\psi - (1 - i\varepsilon_1)N_e(\psi)\psi + i\varepsilon_2|\psi|^4\psi = 0 \tag{5.8}$$

$$\frac{\partial N_e}{\partial t} = |\psi|^6 - N_e^2 - \nu N_e \tag{5.9}$$

where $\varepsilon_1 = 2.36 \times 10^{-6}$ and $\varepsilon_2 = 5.32 \times 10^{-5}$.

To check the spatiotemporal instability result, the initial conditions are taken to be the same as from the previous section which are then perturbed by a 1% random noise in temporal direction.

Figures (5.10) – (5.13) show the propagation of the pulse profile and the fluence of the pulse which corresponds to the energy per unit area. Fluence is computed numerically in the following way:

$$F(x, y, z) = \int_{-\infty}^{\infty} |\psi(x, y, z, t)|^2 dt \tag{5.10}$$

This simulation confirms the theoretical prediction that the pulse of the order of nanoseconds suffers from the modulational instability. Temporal perturbations become significant after several meters. Collapse event accelerates the noise growth. It was observed that beams with less intensity have longer unaffected propagation, since the collapse event develops longer.

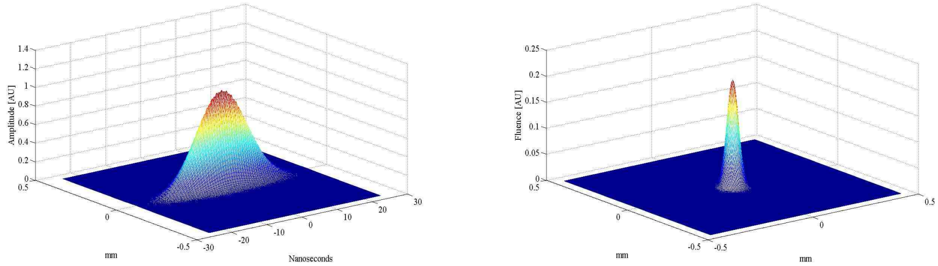

(a) z=0 m (b) z=0 m

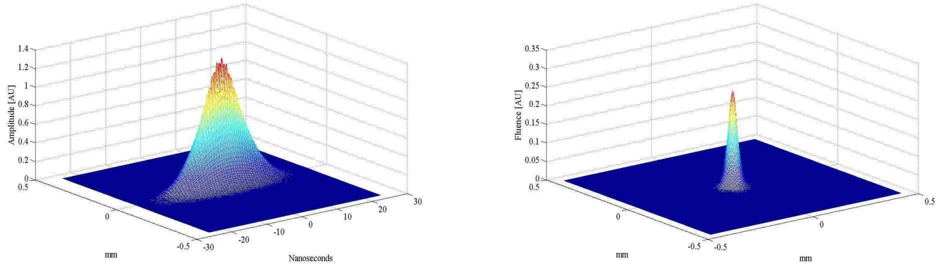

(c) z=1.25 m (d) z=1.25 m

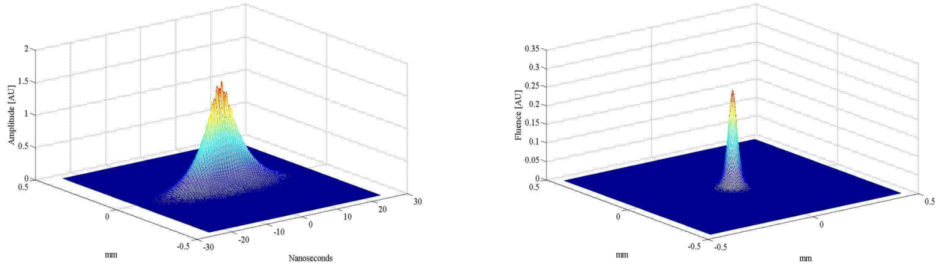

(e) z=2 m (f) z=2 m

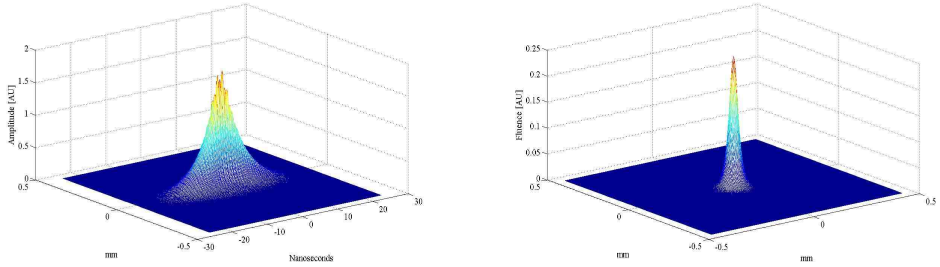

(g) z=2.5 m (h) z=2.5 m

Figure 5.10: Propagation of 10 nanosecond pulse(left column) and fluence(right column)

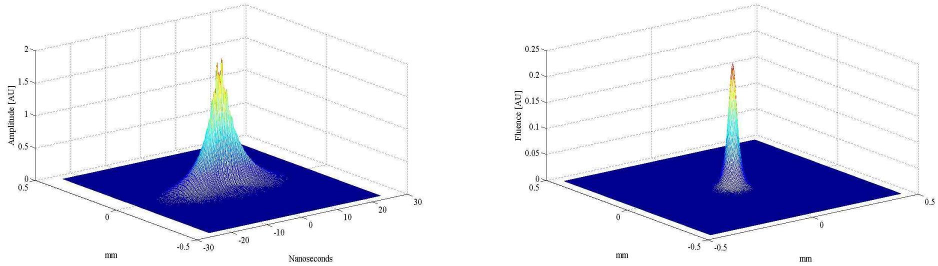

(a) z=3 m (b) z=3 m

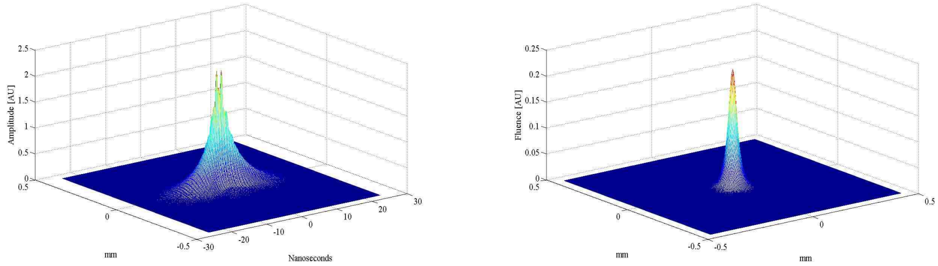

(c) z=3.5 m (d) z=3.5 m

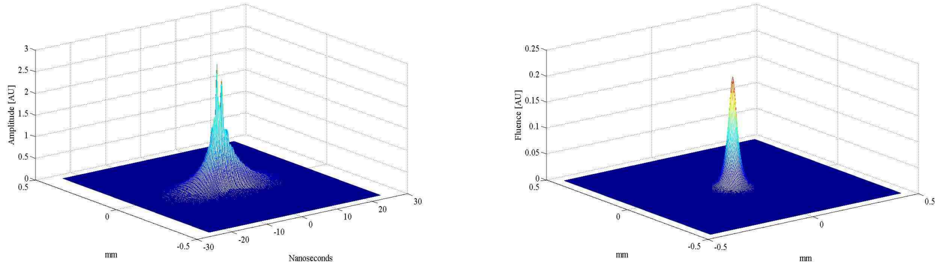

(e) z=4 m (f) z=4 m

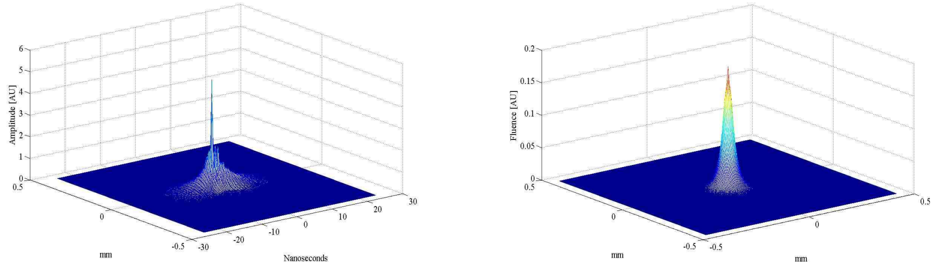

(g) z=4.5 m (h) z=4.5 m

Figure 5.11: Propagation of 10 nanosecond pulse(left column) and fluence(right column)

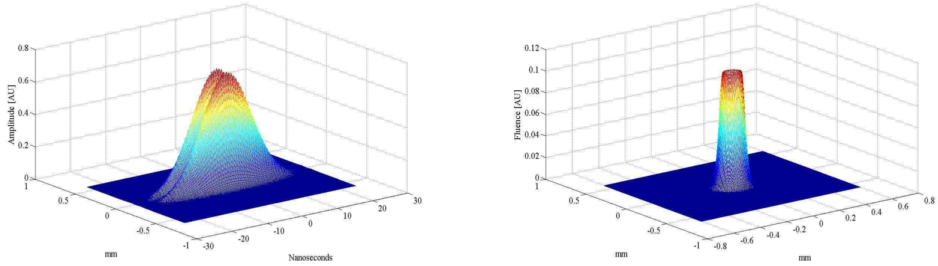

(a) z=0 m

(b) z=0 m

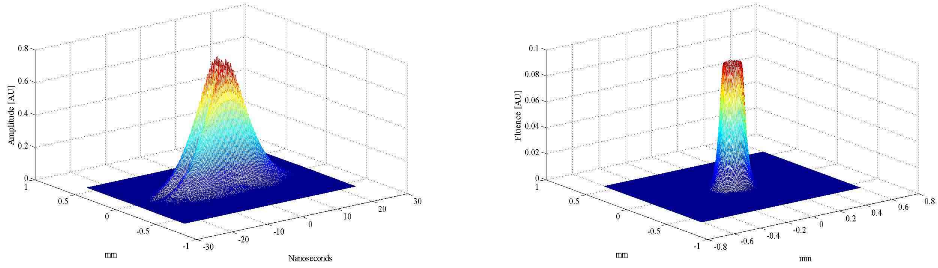

(c) z=5.47 m

(d) z=5.47 m

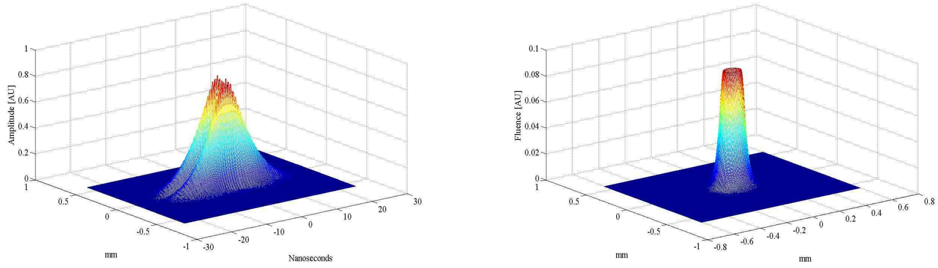

(e) z=7.3 m

(f) z=7.3 m

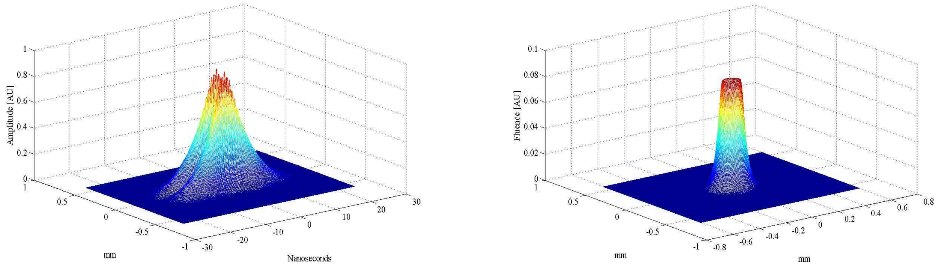

(g) z=9.1 m

(h) z=9.1 m

Figure 5.12: Propagation of 10 nanosecond m=1 vortex pulse(left column) and fluence(right column).

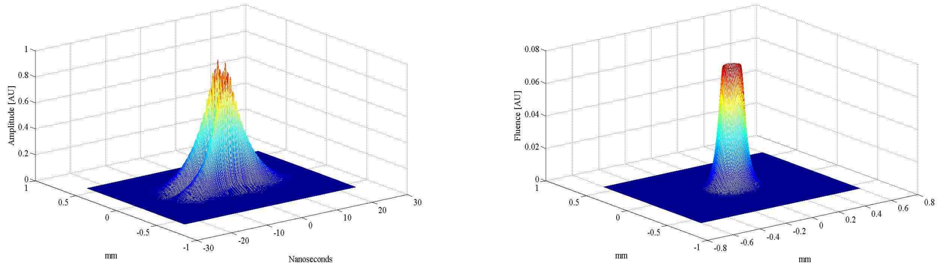

(a) z=10.94 m (b) z=10.94 m

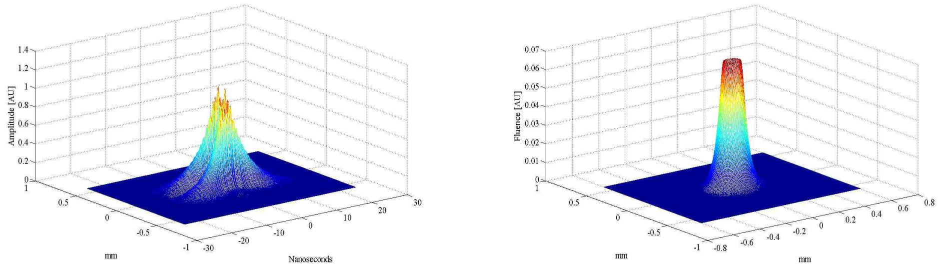

(c) z=12.76 m (d) z=12.76 m

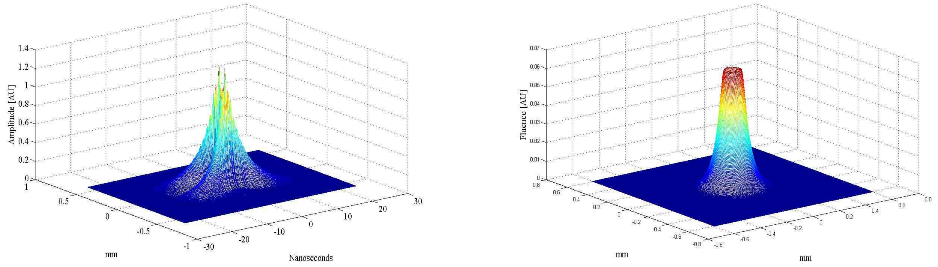

(e) z=14.58 m (f) z=14.58 m

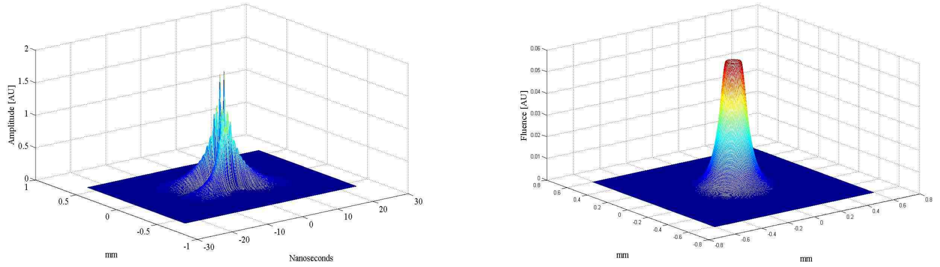

(g) z=16.4 m (h) z=16.4 m

Figure 5.13: Propagation of 10 nanosecond m=1 vortex pulse(left column) and fluence(right column).

Chapter 6

Conclusion

This dissertation studies the theoretical possibility of the propagation of high intensity UV filaments and vortices in air. The governing system of equations were derived and non-dimentionalized. It was shown by Newton's iteration method that the steady state model produces localized radially symmetric solutions for certain range of eigenvalues Λ. It was observed that fundamental stationary solutions can be well approximated by elementary functions, for example in the case of $m = 0$ they can be approximated by gaussian.

The stability of obtained stationary solutions is divided into two parts. First we use semi-analytical approach to study the dynamics of the beam width. The results show stable although oscillatory behavior of the stationary solutions. Then, the linear stability of the radial profiles is investigated. In this case, it was proven by Vakhitov-Kolokolov criterion that the fundamental as well as vortex steady state solutions are stable against spatial perturbations. It was shown that vortex solutions suffer from instability against azimuthal perturbations. In the last part of the chapter 4, spatiotemporal perturbations were applied to full time dependent problem. Analysis of the spectral problem shows that the equilibria of the given model are inherently unstable against temporal perturbations.

Theoretical predictions are consistent with the numerical simulations only if the model assumes long enough pulse to be considered as a continuous wave. Based on the above analysis, the given model predicts that it's possible for UV filaments and vortices to propagate over several meters, even tens of meters before the modulational instability becomes significant to affect the propagation.

Appendix A

Numerical integration scheme

For simulations along the propagation direction a split-step spectral method is used. To describe this method it is convenient to consider the field equation in the following form

$$\frac{\partial\psi}{\partial z} = iL(\psi)\psi + iN(\psi)\psi \tag{A.1}$$

where $L(\psi)$ is a linear part of the equation, and $N(\psi)$ is nonlinear. The field advances from one propagation step to another according to the following expression

$$\psi(\cdot, z + \Delta z) \approx \exp(i\Delta z(L + N(\psi)))\psi(\cdot, z). \tag{A.2}$$

There exists several different splitting procedures of the right-hand side of (A.2). The approach is chosen to be of the second order of accuracy which was introduced by Strang [57].

$$\exp(i\Delta z(L + N(\psi))) \approx \exp(i\Delta zL/2)\exp(i\Delta zN(\psi))\exp(i\Delta zL/2). \tag{A.3}$$

In the obtained expression the linear operator is calculated in the Fourier domain, while the operator $N(\psi)$ is computed in the xy-space.

Although the given model assumes no boundaries in the transverse directions it is unrealistic computationally. Therefore finite boundaries of the same size are imposed in both directions. Define l to be a length of the computational domain. Then the interval $[-l/2, l/2]$ is divided into m equal parts with the spacing $h = l/m$, making grid discretization uniform. In the formula (A.3) the nonlinear operator does not contain any derivatives meaning that the computation is direct on the grid points and no further approximation is needed. The transverse Laplacian in frequency domain is found by utilizing Fast Fourier Transform. The discretization of the spectral grid is also uniform with grid spacing given by $2\pi/(mh)$.

The scheme of the split-step spectral method is given below

```
Step1. Let $\psi^0$ be the input field.
Step2. Find the Fourier transform $\hat{\psi}^0$.
start of the loop
    Step3. $\hat{\psi}^*(\omega_{1j}, \omega_{2k}) = \exp(-i\Delta z(\omega_{1j}^2 + \omega_{2k}^2)/2)\hat{\psi}^n(\omega_{1j}, \omega_{2k})$
    Step4. $\psi^{**}(x_j, y_k) = \exp(i\Delta z N(\psi^*))\psi^*(x_j, y_k)$
    Step5. $\hat{\psi}^{n+1}(\omega_{1j}, \omega_{2k}) = \exp(-i\Delta z(\omega_{1j}^2 + \omega_{2k}^2)/2)\hat{\psi}^{**}(\omega_{1j}, \omega_{2k})$
end
Step6. Find the inverse Fourier transform $\psi^{n_{final}}$
```

where $x_j = jh$, $j = -m/2, ..., m/2-1$, $y_k = kh$, $k = -m/2, ..., m/2-1$, $w_{1j} = 2j\pi/(mh)$, $j = -m/2, ..., m/2-1$, $w_{2k} = 2k\pi/(mh)$, $k = -m/2, ..., m/2-1$.

To achieve the required accuracy, the split-step method requires the following condition to be satisfied [58]

$$\Delta z \leq \frac{2h^2}{\pi^2}. \tag{A.4}$$

References

[1] G. Mourou. The ultrahigh-peak-power laser: present and future. *Appl. Phys. B 65, 205211, 1997.*

[2] D. Strickland, G. Mourou. Compression of amplified chirped optical pulses. *Optic Communications, vol. 56, No. 3, Dec. 1, pp. 219-221, 1985.*

[3] P. Maine, D. Strickland, P. Bado, M. Pessot, G. Mourou. Generation of ultrahigh peak power pulses by chirped pulse amplification. *IEEE J. Quantum Electron. 24, 398-403, 1988.*

[4] A. Braun, G. Korn, X. Liu, D. Du, J. Squier, G. Mourou. Self-channeling of high-peak-power femtosecond laser pulses in air. *Opt. Lett. 20(1), 73-75, 1995.*

[5] A. Brodeur, C. Chen, C. Ilkov, S. Chin, O. Kosareva, V. Kandidov. Moving focus in the propagation of ultrashort laser pulses in air. *Opt.Lett. 22(5), 304-306, 1997.*

[6] E. Nibbering, P. Curley, G. Grillon, B. Prade, M. Franco, F. Salin, A. Mysyrowicz. Conical emission from self-guided femtosecond pulses in air. *Opt. Lett. 21(1),62-64, 1996.*

[7] Z. Jin, J. Zhang, M.H. Lu, Y.T. Li, Z.H. Wang, Z.Y. Wei, X.H. Yuan, W. Yu. Control of filamentation induced by femtosecond laser pulses propagating in air. *Optics Express 10424, Vol. 13, No. 25, Dec. 2005.*

[8] Z-Q Hao, J. Zhang, X. Lu, T-T Xi, Y-T Li, X-H Yuan, Z-Y Zheng, Z-H Wang, W-J Ling, Z-Y Wei. Spatial evolution of multiple filaments in air induced by femtosecond laser pulses. *Optics Express 773, Vol. 14, No. 2, Jan 2006.*

[9] V. Talanov. Self-focusing of electromagnetic waves in nonlinear media. *Izv. Vysshikh Uchebn. Zavedenii Radiofiz 7, 564-565, 1964.*

[10] V. Talanov Self-focusing of wave beams in nonlinear media. *JETP Lett. 2(5), 138, 1965.*

[11] J.Kasparian, J-P Wolf. Physics and applications of atmospheric nonlinear optics and filamentation. *Optics express 466, Vol. 16, No. 1, 2008.*

[12] A. Couairon, A. Mysyrowicz. Femtosecond filamentation in transparent media. *Physics Reports 441, 47 189, 2007.*

[13] L. Berge. Wave collapse in physics: principles and applications to light and plasma waves. *Physics Reports, 303:259370, 1998.*

[14] K.D. Moll, A.L. Gaeta, G. Fibich. Self-Similar Optical Wave Collapse: Observation of the Townes Profile. *Physical Review Letters, Vol. 90, No. 20, May 2003.*

[15] Gadi Fibich, Shmuel Eisenmann, Boaz Ilan, Yossi Erlich, Moshe Fraenkel, Zohar Henis, Alexander L. Gaeta and Arie Zigler. Self-focusing distance of very high power laser pulses. *Optics Express Vol. 13, No. 15, 5898, 25 July 2005.*

[16] J-C Diels, W. Rudolph. Ultrashort Laser Pulse Phenomena. *Second Edition, Academic Press, 2006.*

[17] A. Couairon, L. Berge. Light filaments in air for ultraviolet and infrared wavelength. *Physical Review Letters, 88(13):135003, Mar 2002.*

[18] E. Arevalo. Self-focusing arrest of femtosecond laser pulses in air at different pressures. *Physical Review E 74, 016602, 2006.*

[19] M. Mlejnek, E.M. Wright, J.V. Moloney. Dynamic spatial replenishment of femtosecond pulses propagating in air. *Optics Letters 382, Vol. 23, No. 5, March 1998.*

[20] V. Skarka, N.B. Aleksic, V.I. Berezhiani. Evolution of singular optical pulses towards vortex solitons and filamentation in air. *Physics Letters A, p.1-8, Oct. 2003.*

[21] A. Vincotte and L. Berge, Femtosecond Optical Vortices in Air. *Phys. Rev. Lett. 95, 193901, 2005.*

[22] M. Kolesik, J. Moloney. Self-healing femtosecond light filaments. *Opt. Lett. 29(6), 590-592, 2004.*

[23] F. Courvoisier, V. Boutou, J. Kasparian, E. Salmon, G. Mejean, J. Yu, J. Wolf. Ultraintense light filaments transmitted through clouds. *Appl. Phys. Lett. 83(2), 213-215, 2003.*

[24] A. Dubietis, E. Kucinskas, G. Tamosauskas, E. Gaizauskas, M. Porras, P. Di Trapani. Self-reconstruction of light filaments. *Opt. Lett. 29, 2893-2895, 2004.*

[25] G. Mechain, C. D'Amico, Y. Andre, S. Tzortzakis, M. Franco, B. Prade, A. Mysyrowicz, A. Couairon, A. Salmon, R. Sauerbrey. Length of plasma filaments created in air by a multiterawatt femtosecond laser. *Opt. Commun. 247,171-180, 2005.*

[26] G. Matvienko, V. Veretennikov, G. Krekov, M. Krekova. Remote sensing of atmospheric aerosols with a white-light femtosecond lidar. *Atmos. Oceanic Opt. 16, 1013-1019, 2003.*

[27] E. Frejafon, J. Kasparian, P. Rambaldi, B. Vezin, V. Boutou, J. Yu, M. Ulbricht, D. Weidauer, B. Ottobrini, E. de Saeger, B. Kramer, T. Leisner, P. Rairoux, L. Woste, J-P Wolf. Laser applications for atmospheric pollution monitoring. *Eur. Phys. J. D 4, 231, 1998.*

[28] J. Kasparian, M. Rodriguez, G. Mejean, J. Yu, E. Salmon, H. Wille, R. Bourayou, S. Frey, Y-B Andre, A. Mysyrowicz, R. Sauerbrey, J-P Wolf, L. Woste. White light filaments for atmospheric analysis. *Science 301,61, 2003.*

[29] K. Stelmaszczyk, P. Rohwetter, G. Mejean, J. Yu, E. Salmon, J. Kasparian, R. Ackermann, J-P Wolf, L. Woste. Long-distance remote laser-induced breakdown spectroscopy using filamentation in air. *Appl. Phys.Lett. 85(18), 3977-3979, 2004.*

[30] P. Rohwetter, J. Yu, G. Mejean, K. Stelmaszczyk, E. Salmon, J. Kasparian, J-P Wolf, L. Woste. Remote LIBS withultrashort pulses: characteristics in picosecond and femtosecond regimes. *J. Anal. At. Spectrom. 19, 437-444, 2004.*

[31] Xin Miao Zhao, Jean-Claude Diels, Cai Yi Wang, and Juan M. Elizondo. Femtosecond ultraviolet laser pulse induced lightning discharges in gases. *IEEE Journal of Quantum Electronics, 31:599612, 1995.*

[32] P. Rambo, J. Schwarz, J-C Diels. High-voltage electrical discharges induced by an ultrashort-pulse UV laser system. *J. Opt. A: Pure Appl. Opt. 3 146-158, 2001.*

[33] C.Sulem, P.L.Sulem. The Nonlinear Scrodinger Equation, Self-focusing and Wave Collaspe. *Applied Mathematical Science, Springer-Verlag, New York Inc, 1999.*

[34] J. Schwarz, P. Rambo, J-C Diels, M. Kolesik, E. Wright, J. Moloney. Ultraviolet filamentation in air. *Optics Comm. 180, 383-390, 2000.*

[35] J. Schwarz, J-C Diels. Analitical solution for uv filaments. *Physical Review A, vol. 65, 013806, 2001.*

[36] O. Chalus, A. Sukhinin, A. Aceves, J-C Diels. Propagation of non-diffraction intense ultraviolet beams. *Optics Communications 281, 3356-3360, 2008.*

[37] R.W. Boyd. Nonlinear Optics, Second Edition. *Academic Press, 2003.*

[38] Y. Shen. The Principles of Nonlinear Optics. *Wiley-Interscience, New York, 1984.*

[39] N.N. Akhmediev, A. Ankiewicz. Solitons, Nonlinear pulses and beams. *Chapman & Hall, 1997.*

[40] Y.S. Kivshar, G.P. Agrawal. Optical Solitons, From Fibers to Photonic Crystals. *Academic Press, 2003.*

[41] A. Couairon, L. Berge. Modeling the filamentation of ultra-short pulses in ionizing media. *Physics of Plasmas, Vol. 7, No. 1, Jan. 2000.*

[42] S.Skupin, L.Berge. Self-guiding of femtosecond light pulses in condensed media: Plasma generation versus chromatic dispersion. *Physica D 220, 14-30, 2006.*

[43] G. Fibich, G. Papanicolaou. Self-focusing in the perturbed and unperturbed nonlinear Schrodinger equation in critical dimension. *SIAP Volume 60 Issue 1, Pages 183-240, Society for Industrial and Applied Mathematics, 1999.*

[44] W. H. Press, S. A. Teukolsky, W. T. Vetterling, B. P. Flannery. Numerical Recipes 3rd Edition: The Art of Scientific Computing. *Cambridge University Press, 2007.*

[45] D. Anderson. Variational approach to nonlinear pulse propagation in optical fibers. *Physical Review A, 27:31353145, 1983.*

[46] D. Anderson, M. Bonedal. Variational approach to nonlinear self-focusing of Gaussian laser beams. *Physics of Fluids, 22(1), p.1838, 1979.*

[47] D. Anderson, M. Lisak, A. Berntson. A variational approach to nonlinear evolution equations in optics. *Pramana-journal of physics, Vol. 57, Nos 5 & 6, pp. 917-936, Nov. & Dec. 2001.*

[48] N.G. Vakhitov, A.A. Kolokolov. Stationary solutions of the wave equation in a medium with nonlinearity saturation. *Radiophys. and Quantum Electronics 16, 783-789, 1973.*

[49] M.I. Weinstein. Modulational stability of ground-states of nonlinear Scrodinger-equations. *SIAM Jouranl on Mathematical Analysis, 16(3):472-491, 1985.*

[50] M.I. Weinstein. Lyapunov stability of ground-states of nonlinear dispersive evolution-equations. *Communications on Pure and Applied Mathematics, 39(1):51-67, 1986.*

[51] E. Kuznetsov, A. Rubenchik, V. Zakharov. Soliton stability in plasmas and hydrodynamics. *Physics Report 142, No. 3, 103-165, 1986.*

[52] R. Caplan, Q. Hoq, R. Carretero-Gonzalez, P. Kevrekidis. Azimuthal modulational instability of vortices in the nonlinear Schrodinger equation. *Optics Communications 282 1399-1405, 2009.*

[53] D. Pelinovsky, R. Grimshaw. Asymptotic methods in soliton stability theory. Nonlinear instability analysis. *Advances in Fluid Mechanics. Vol. 12, p. 245-312, 1997.*

[54] V. Zakharov. Instability of Self-focusing of Light. *Soviet Physics JETP, Vol. 26, p.994.*

[55] T. A. Niday, E. M. Wright, M. Kolesik, and J. V. Moloney. Stability and transient effects for nanosecond ultraviolet light filament in air. *Phys. Rev. E, 72, 016618, 2005.*

[56] V. Tikhonenko, J. Christou, and B. Luther-Daves. Spiraling bright spatial solitons formed by the breakup of an optical vortex in a saturable self-focusing medium. *J. Opt. Soc. Am. B /Vol. 12, No. 11 /November 1995.*

[57] G. Strang, On the construction and comparison of difference schemes. *SIAM J. Numer. Anal. 5 (3) (1968) 506517.*

[58] J. A. C. Weideman, B. M. Herbst. Split-Step Methods for the Solution of the Nonlinear Schrodinger Equation. *SIAM Journal on Numerical Analysis, Vol. 23, No. 3 pp. 485-507, 1986.*